



HAL
open science

Numerical modelling of the muddy layer effect on Ship's resistance and squat

Sami Kaidi, Emmanuel Lefrançois, Hassan Smaoui

► To cite this version:

Sami Kaidi, Emmanuel Lefrançois, Hassan Smaoui. Numerical modelling of the muddy layer effect on Ship's resistance and squat. *Ocean Engineering*, 2020, 199, pp.106939. 10.1016/j.oceaneng.2020.106939 . hal-02464217

HAL Id: hal-02464217

<https://utc.hal.science/hal-02464217v1>

Submitted on 7 Mar 2022

HAL is a multi-disciplinary open access archive for the deposit and dissemination of scientific research documents, whether they are published or not. The documents may come from teaching and research institutions in France or abroad, or from public or private research centers.

L'archive ouverte pluridisciplinaire **HAL**, est destinée au dépôt et à la diffusion de documents scientifiques de niveau recherche, publiés ou non, émanant des établissements d'enseignement et de recherche français ou étrangers, des laboratoires publics ou privés.



Distributed under a Creative Commons Attribution - NonCommercial 4.0 International License

1 **NUMERICAL MODELLING OF THE MUDDY LAYER EFFECT ON SHIP'S RE-**
2 **SISTANCE AND SQUAT**

3

4 **Sami Kaidi**, CEREMA-DtecEMF, Margny les Compiègne, France ;

5 **Emmanuel Lefrançois**, Université de technologie de Compiègne Sorbonne universités, laboratoire Roberval FRE 2012
6 CNRS, France ;

7 **Hassan Smaoui**, CEREMA-DtecEMF, Margny les Compiègne, France ;

8

9 **ABSTRACT**

10 The increasing use of maritime transport has led to an increase in ship size. However, the dimensions of channels and
11 harbours cannot follow the expansion rate of ships. Large ships will experience shallow water effects such as the bottom
12 effect more severely, which plays an important role in the manoeuvrability and the stability of ships. To reduce naviga-
13 tional restriction in estuary environment and close to ports (see Figure 1), the World Association for Waterborne
14 Transport Infrastructure (PIANC) established the concept of the nautical bottom. Using this concept, ships can navigate
15 with both small and negative under keel clearance (UKC) relative to the water-mud interface. Hence, the aim of this
16 work, is to conduct a numerical investigation in order to study the influence of the muddy seabed on the ship's manoeu-
17 vrability especially on the ship's resistance and squat. Accordingly, a 3D Computational Fluid Dynamics (CFD) model
18 based on the Volume of Fluid (VoF) method was used to simulate the multiphase flow for various setups. Four parame-
19 ters were tested: the mud properties, the ship's speed, the mud thickness and the UKC value relative to the water-mud
20 interface. The numerical results of this investigation were in reasonable agreement with experimental data. Through this
21 investigation it was also shown the performances of the CFD method to simulate setups difficult to achieve in towing
22 tank.



23

24

Figure 1. Ship sailing in the Gironde estuary.25 **NOMENCLATURE**

α_p	<i>Volume fraction</i>
B	<i>Ship's beam (m)</i>
C_B	<i>Ship's block coefficient</i>
Fn	<i>Froude number</i>
Fn_i	<i>Internal Froude number</i>
h	<i>Total depth (m) (water + mud)</i>
h_w	<i>Water depth (m)</i>
h_m	<i>Mud thickness (m)</i>
K	<i>Consistency factor (Kg.sⁿ.2/m)</i>
L_{OA}	<i>Ship's Length over all (m)</i>
L_{PP}	<i>Ship's length between perpendiculars (m)</i>
n	<i>Power law exponent</i>
T	<i>Ship's draft (m)</i>
t	<i>Time (s)</i>
p	<i>Fluid pressure (Pa)</i>
p'	<i>Fluctuation of the fluid pressure (Pa)</i>
UKC	<i>Under Keel Clearance (m)</i>
\mathbf{u}	<i>Fluid velocity vector (m/s)</i>
\mathbf{u}'	<i>Fluctuation of the fluid velocity vector (m/s)</i>
V_s	<i>Ship speed (m/s)</i>
η	<i>Dynamic viscosity (Pa.s)</i>
ρ_w	<i>Water density (kg/m³)</i>
ρ_m	<i>Mud density (kg/m³)</i>
$\dot{\gamma}$	<i>Shear rate (1/s)</i>
$\dot{\gamma}_c$	<i>Critical shear rate (1/s)</i>
τ	<i>Shear stress (Pa)</i>
τ_0	<i>Yield stress (Pa)</i>

26 **1 INTRODUCTION**

27

28 Any ship navigating through confined and shallow waters is strongly affected by hydrodynamic effects, as opposed to in
 29 open seas. Major effects of the limited navigating width and water depth (h) are the squat effect, and the increase in the
 30 ship's resistance. Water in front of the bow is pushed away, and flows down to the sides and under the hull of the ship
 31 with an increased velocity (See Figure 2) due to the reduced section. According to Bernoulli's principle, increasing ve-
 32 locity under the hull indicates a vertical pressure drop, and consequently the ship's sinkage increases. In addition, the
 33 ship generally trims forward or aft, as the bow or stern may experience more or less pressure drop, depending on the ship
 34 type. The effects of sinkage and trim are known as the ship's squat. This has a significant influence on the ship's re-
 35 sistance and can lead to serious safety issues, such as grounding, loss of steering, or collision.

36

37 In estuaries, the presence of the mud layer can significantly modify the ship's behaviour, especially when the ship is
 38 navigating in negative UKC relative to the mud/water interface. Note that the concept of the nautical bottom was estab-
 39 lished by the PIANC MarCom Working Group 30 in their 2014 report. This concept enables ships with larger drafts

40 whose physical properties do not exceed the critical limit (whereby contact with the ship's keel causes damage or unac-
41 ceptable effects on controllability and manoeuvrability) to navigate in the mud layer. The same report also noted that it
42 is difficult to give the critical limit value, hence, different density limits were set for different ports. That said, a critical
43 limit was still provided, based only on the mud density, where the nautical bottom is the level from where the mud den-
44 sity is more than 1200 kg/m^3 . The viscosity of the mud could not be used as a parameter to define the nautical bottom
45 because it changes under shear rates change. In some ports, such as the Port of Emden, Germany, the critical limit is
46 given as a yield point that has been fixed to 100 Pa (Wurpts, 2005). Using this criterion, it was observed that the corre-
47 sponding bottom density (approximately 1300 kg/m^3) considerably exceeded the limit given by PIANC.

48

49 In the Gironde estuary, the squat is an essential parameter for the traffic management of ships, where the water level in
50 the estuary depends on the tide. Accordingly, to accommodate larger ships it is necessary to wait until the tide is high.
51 Ships have to sail at the same speed as the propagation of the tide wave, which is in the order of 10 kn . However, this is
52 not always the case, because in some situations ships can no longer keep up with the speed of the tidal wave for various
53 reasons (mainly related to the significant increase in the ship's resistance caused by the ship's squat in the mud, which
54 slows its speed considerably). In other situations, ships are equipped with a power limiter that stops the operation of the
55 propulsive system if the ship meets a strong resistance. In such a situation, ships will be moored to wait for the next tide.
56 To manage the estuarine network better, and to ensure safe navigation, it is thus essential to study the phenomenon of
57 ship's resistance, its origins, and any consequences for navigation.

58 To predict a ship's squat, several empirical formulas have previously been proposed. Barrass and Derrett (1999) con-
59 cluded some important factors of the squat effect, as follows:

- 60 • The main factor is the ship speed relative to the water, and the squat is approximately proportional to the square of
61 this velocity;
- 62 • The decrease of water depth will increase the ship's squat;
- 63 • The block coefficient of the ship (that is the ratio of the ship's underwater volume to the volume of box surrounding
64 it) is proportional to the squat;
- 65 • Similarly, the blockage factor (a ratio of the ship's immersed cross section to that of the canal) has a direct impact
66 on the squat.

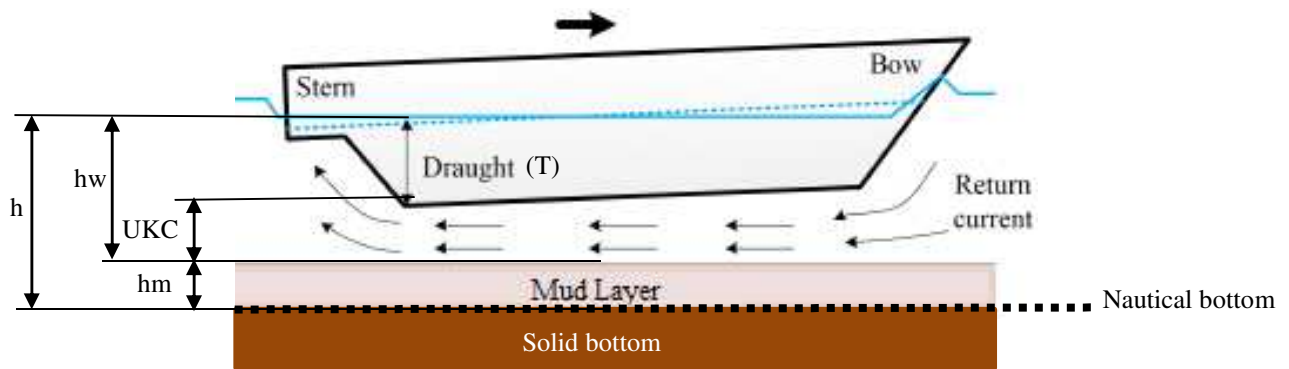


Figure 2. Nautical bottom representation with flow around a ship.

67

68

69

70

71

72

73

74

75

76

77

78

79

80

81

82

83

84

85

86

87

88

89

90

91

Over time, numerical efforts have been focused on estimating ship's resistance and squat. The slender-body method assumes that a ship's beam, free surface wave amplitude, and water depth are small compared to its length. This allows the simplification of the flow simulation in two dimensions using the slender-body theory (Gourlay, 2008; Tuck, 1964). To take into account the dynamic coupling of a ship's motion with flow, the potential flow theory can be applied, which only assumes the flow to be irrotational. This has been widely used for squat prediction and very good results have been obtained (Debaillon, 2010; Ma et al., 2016; Sergent et al., 2015), whereas it is difficult to apply the potential flow model to resistance prediction, because it neglects the viscous stresses, crucial for evaluating the ship's resistance.

Modern CFD techniques based on solving the fully viscous Navier-Stokes equations have been extensively applied to ship hydrodynamics with fruitful results, as they consider the important features of the actual flow, such as viscous effects and turbulence. Hence, they are more reliable for predicting ship's resistance and motions. (Stern, 2013) summarised the achievements made regarding ship hydrodynamics using CFD in the last decade. Further, recent progress in modern computational ship hydrodynamics with respect to shallow and confined water has been made. (Elout et al., 2015) performed a turning circle and a zigzag test on a KVLCC2 hull model to determine the manoeuvring performance in a shallow water zone. To study the scale effect, (Tezdogan et al., 2016) performed unsteady Reynolds-averaged Navier-Stokes (RANS) simulations at full-scale for the squat in shallow water with STAR-CCM+ commercial software. They compared the results to the 3D potential flow theory and the experimental data of Mucha et al. (2014). They reported an underestimation of the ship squat and pointed indicated that the ship's resistance is sensitive to sinkage. (Linde et al., 2016) validated this observation with FLUENT, by simulating the ship's resistance both with and without consideration of ship sinkage. The predicted value of resistance with sinkage was closer to the experimental data. (Kaidi et al.,

92 2017) further studied the ship manoeuvring with FLUENT under the effect of bank-propeller hull interaction in shallow
93 water.

94

95 In ports, flow stratification might occur as the non-saline, light river water flows into the colder and heavier saline sea-
96 water, leading to large horizontal or vertical fluid density variations. Highly density-stratified waters are known to pose
97 particular challenges to navigating ships. When a ship's keel (bottom) is travelling just above the interface of the water
98 layers, the ship experiences large wave resistance. This resistance occurs particularly if the ship is travelling close to the
99 speed of the fastest internal waves, due to the generation of large internal waves. This phenomenon, known as 'dead
100 water', affects the ability of ships to move through stratified water. Accurately assessing the effects of stratified flow on
101 ship navigation requires a detailed knowledge of the flow field, including turbulent mixing and in particular, the genera-
102 tion of internal waves on the interface between the two layers of water.

103

104 Crapper (1967) and Hudimac (1961) presented analytical approaches to study the internal wave modes caused by a mov-
105 ing body in a two-layered ocean. It follows from their work that—just as for surface waves—at ship speeds sufficiently
106 larger than the internal wave speed, only divergent waves travel downstream from the ship, while both divergent and
107 transverse waves are present for slower ships. (Tulin et al., 2000) suggested a nonlinear theory to capture internal wave
108 behaviour at high Froude number (Fn) in weakly stratified flow, which compared satisfactorily with available experi-
109 mental results for a semi-submerged spheroid. (Delefortrie et al., 2004; Delefortrie and Vantorre, 2005) conducted a
110 large number of experiments on towing tanks. They studied the mud layer effect on the ship manoeuvring by considering
111 several parameters. They also developed a mathematical model to take into account the mud effect. (Chang et al., 2006)
112 presented one of the few available examples of the use of CFD for a ship in a stratified medium. (Esmailpour et al.,
113 2016) studied the evolution of the stratified flow in the near field of a surface ship in detail. They demonstrated that the
114 generation of internal waves requires energy, which results in an increase in resistance.

115

116 In this paper, we present an overview of a numerical study of the mud layer effect on ship's resistance and sinkage by
117 using a multi-phased CFD method. Note that, the mud is supposed stratified, hence, the water and the mud were mod-
118 elled as separate layers with average values of density and viscosity. The main objective of this work is to test the ability
119 of the CFD method to simulate and assess the influence of the mud on the hydrodynamic forces acting on the ship's hull.
120 Four parameters were tested: the mud properties, the ship speed (V_s), the mud thickness and the UKC. A preliminary
121 study was conducted to first show the influence of the non-Newtonian behaviour of mud on the ship's resistance, and the

122 internal waves at the mud-water interface. Based on this preliminary study, the Newtonian model was selected for this
 123 investigation. The UKC level was referenced to the water-mud interface; hence, it can take both positive and negative
 124 values. The limits of the CFD method are discussed in Section 5.

125

126 **2 MATHEMATICAL FORMULATION AND NUMERICAL METHODS**

127

128 The fluid flow is governed by the incompressible viscous Navier-Stokes equations completed with the continuity equa-
 129 tion, as follows:

$$130 \quad \nabla \cdot \mathbf{u} = 0 \quad (1)$$

$$131 \quad \frac{\partial \mathbf{u}}{\partial t} + \nabla \cdot (\mathbf{u} \otimes \mathbf{u}) = -\frac{1}{\rho} \nabla p + \frac{\eta}{\rho} \nabla^2 \mathbf{u} \quad (2)$$

132

133 where \mathbf{u} and p represent the velocity vector and pressure, respectively, and ρ and ν are the fluid properties of density and
 134 kinematic viscosity.

135

136 2.1 TURBULENCE MODELLING

137

138 To model the turbulence effect, the Reynolds averaging was computed on the flow variable in time, which gave rise to

139

$$140 \quad \nabla \cdot \mathbf{U} = 0 \quad (3)$$

$$141 \quad \frac{\partial \mathbf{u}}{\partial t} + \nabla \cdot (\mathbf{U} \otimes \mathbf{U}) = -\frac{1}{\rho} \nabla p + \frac{\eta}{\rho} \nabla^2 \mathbf{U} - \nabla \cdot (\mathbf{u}' \otimes \mathbf{u}') \quad (4)$$

142

143 where $\mathbf{u} = \mathbf{U} + \mathbf{u}'$ and $p = P + p'$. The last term in the RANS momentum equation is the Reynolds stress, which is
 144 often approximated by turbulence models. In this research, we employed the *SST k- ω* turbulence model, which is actual-
 145 ly a combination of the *k- ω* and *k- ϵ* models while a shifting function is used to switch one from another.

146 2.2 MULTIPHASE APPROACH

147

148 The volume of fluid (VoF) method was used to simulate three-phase interactions (the interface of air/water and wa-
 149 ter/mud). Using this approach, both interfaces can be captured in a fixed grid by solving the continuity equation of the
 150 volume fraction (Eq. 5), as follows:

151

$$\frac{\partial \alpha_p}{\partial t} + \mathbf{u} \nabla \alpha_p = 0 \quad (p = 1, 2) \quad (5)$$

152

153 α_p denotes the volume fraction of the p^{th} fluid, and:

$$\sum_{p=1}^n \alpha_p = 1 \quad (n = 2 \text{ or } 3) \quad (6)$$

154 Equations presented thus far (Eq. 1–6) are solved using the commercial code Ansys-Fluent 13.0 based on the finite vol-
 155 ume method. The pressure-velocity coupling was ensured by using a steady pressure-based coupled algorithm, and the
 156 interpolation method selected to compute the cell-face pressure was the PREssure STaggering Option (PRESTO). The
 157 second order was set for the VoF's special discretisation.

158 2.3 NON-NEWTONIAN BEHAVIOUR LAW FOR MUD

159

160 It should be noted that mud behaviour is often considered non-Newtonian, which means the viscosity depends on the
 161 shear rate. Hence, the Herschel-Bulkley model was selected to reproduce this behaviour. The Herschel-Bulkley model is
 162 represented by the following equations:

163

$$\tau = \tau_0 + K\dot{\gamma}^n \quad \text{if } \tau > \tau_0 \quad (7)$$

$$\tau = 0 \quad \text{if } \tau \leq \tau_0 \quad (8)$$

164

165 where, τ and τ_0 are shear and yield stress, respectively. K is the consistency factor, n is the power law exponent, and $\dot{\gamma}$ is
 166 the shear rate.

167

168 The non-Newtonian viscosity η is computed using one of the following formulas:

$$169 \quad \eta = \frac{\tau_0}{\dot{\gamma}} + K\dot{\gamma}^{n-1} \quad \text{for } \dot{\gamma} > \dot{\gamma}_c \quad (9)$$

$$170 \quad \eta = \frac{\tau_0 \left(2 - \frac{\dot{\gamma}}{\dot{\gamma}_c}\right)}{\dot{\gamma}} + K\dot{\gamma}_c^{n-1} \left[(2 - n) + (n - 1) \frac{\dot{\gamma}}{\dot{\gamma}_c} \right] \quad \text{for } \dot{\gamma} < \dot{\gamma}_c \quad (10)$$

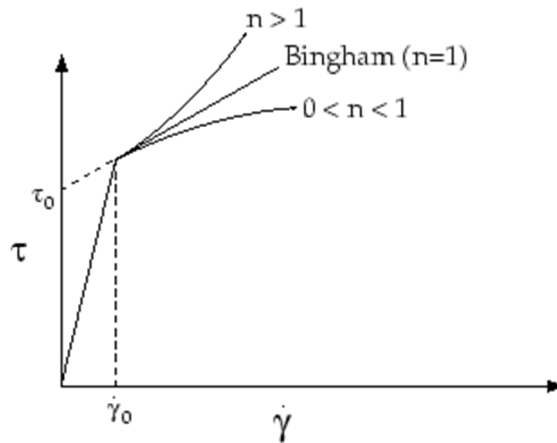
171

172 $\dot{\gamma}_c$ is the critical shear rate.

173

174 Figure 3 shows the variation of the shear stress with shear rate according to the Herschel-Bulkley model.

175



176

177 **Figure 3. Shear stress as a function of the shear rate basing on the Herschel-Bulkley model (This figure was tak-**
 178 **en from the Fluent software manual)**

179

180 2.4 VERIFICATION AND VALIDATION OF THE CFD MODEL

181

182 The procedures for verification and validation of the CFD model have been discussed and performed in several previous
 183 works (Kaidi et al., 2017, 2018; Razgallah et al., 2018; Ali et al., 2018), and were carried out in accordance with the
 184 ITTC recommendations. Verification consisted of tests and analysis of the results of several mesh qualities, whilst vali-
 185 dation was performed by taking the numerical results of the ship's resistance, the profile of generated waves, and the
 186 ship's squat and comparing them to the measurements carried out in a towing tank of the University of Liège and the
 187 Central School of Nantes. Note that no mud layer was considered in these works: only the water-air interface was mod-
 188 elled and validated.

189 Based on the obtained results, it was concluded that the CFD model provided a good estimate of the hydrodynamic forc-
 190 es around the ship's hull, and correctly captured the air-water interface. It was also concluded that the CFD model could
 191 simulate the sediment suspension and transport accurately (Kaidi et al., 2018).

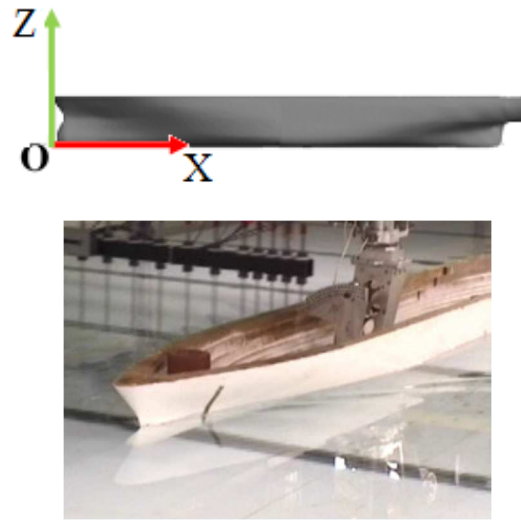
192

193 **3 STUDIED SHIP, CHANNEL CONFIGURATION, BOUNDARY CONDITIONS, AND MUD PROPER-**
 194 **TIES**

195

196 To conduct this investigation, we used a container cargo-hull form (see Figure 4). This kind of ship was selected because
 197 it is one of the most common ships to sail in the Gironde estuary. Table 1 provides the main characteristics of the hull,
 198 where, L_{PP} is the length between perpendicular, L_{OA} is the length over all, B is the ship beam, T is the ship draft, and C_B
 199 is the block coefficient. Note that the same reference frame is used in this investigation. The origin of this reference is

200 fixed on the ship, where the $x = 0$ corresponds to the ship's bow plane, while, the $z = 0$ corresponds to the ship's keel
 201 plane. The X-axis is oriented right while the Z-axis is oriented up as is shown in Figure 4.



202 **Figure 4. Container carrier-hull form.**

203

204 **Table 1. Ship dimensions and scales**

205	Ship	Container cargo	
206	Scale	1/1	1/80
207	L_{PP} (m)	230.0	2.875
208	L_{OA} (m)	232.5	2.906
209	B (m)	32.2	0.402
210	T (m)	10.0	0.125
211	C_B	0.681	0.681

212

213 In the present study, we considered only the confinement effect using the UKC. To prevent large body motions, the
 214 reference frame was fixed on the ship; hence, the fluid and other parts moved relative to the hull. The computational
 215 domain was chosen with a rectangular section, large enough such that there was little influence of the position of the
 216 inlet and outlet: $1-2 L_{pp}$ for the inlet and $3-5 L_{pp}$ for the outlet are recommended by ITTC (ITTC, 2011). Half of the
 217 computational domain was used to reduce computational time.

218

219 For the boundary conditions, at the inlet the flow velocity was imposed, and at the outlet the outflow condition was used.

220 A symmetrical condition was applied at the top, at the mid-plane, and at the side boundaries. At atmosphere, total pres-

221 sure was applied; at the bottom moving wall condition was employed to take into account the relative motion, and at the
222 hull's surface no-slip wall condition was used.

223

224 Four combinations of mud properties were selected to conduct this investigation. These properties represent the average
225 values measured at different zones in the Gironde estuary and some ports. Table 2 presents the combination of the densi-
226 ty and viscosity of the mud.

227

228 **Table 2. Physical properties of tested mud**

Mud type	density (kg/m ³)	viscosity (Pa.s)
Mud A	1085	0.025
Mud B	1160	0.068
Mud C	1210	0.128
Mud D	1230	0.260

234

235 **4 RESULTS AND DISCUSSION**

236

237 4.1 COMPARISON BETWEEN THE NEWTONIAN AND NON-NEWTONIAN MODELS

238 The effect of the use of non-Newtonian viscosity to simulate the mud behaviour is discussed in this section. Using the
239 CFD method, the mud layer could be modelled in different ways. The first was to suppose that the mud properties were
240 constant and slightly influenced by the shear stress induced by the ship's passage. Hence, we used average values for the
241 density and the viscosity. The second was to consider that the mud was significantly affected by the shear stress, from
242 where a non-Newtonian model was used to estimate the dynamic viscosity.

243

244 It should be highlighted that in the estuary environment, the flow was modelled using hydraulic models, which estimate
245 the average turbulent viscosity at the channel bottom that can be used by manoeuvring simulators. This provides indis-
246 pensable results for assessing the difference between the results obtained by both approaches.

247

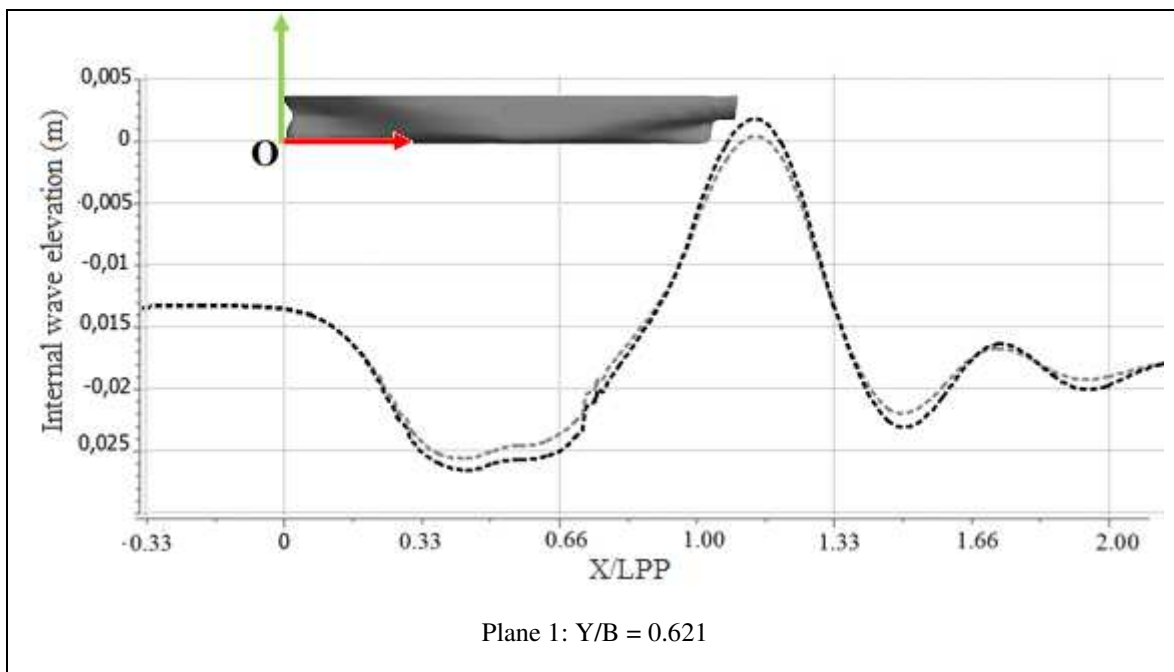
248 To carry out this study, the ship's draft was set to 10 m (0.125 m in the model) and the ship's speed was set to 10 kn
249 (0.575 m/s). The mud thickness used was 3 m in full scale (0.0375 m in the scaled model), which corresponds to the

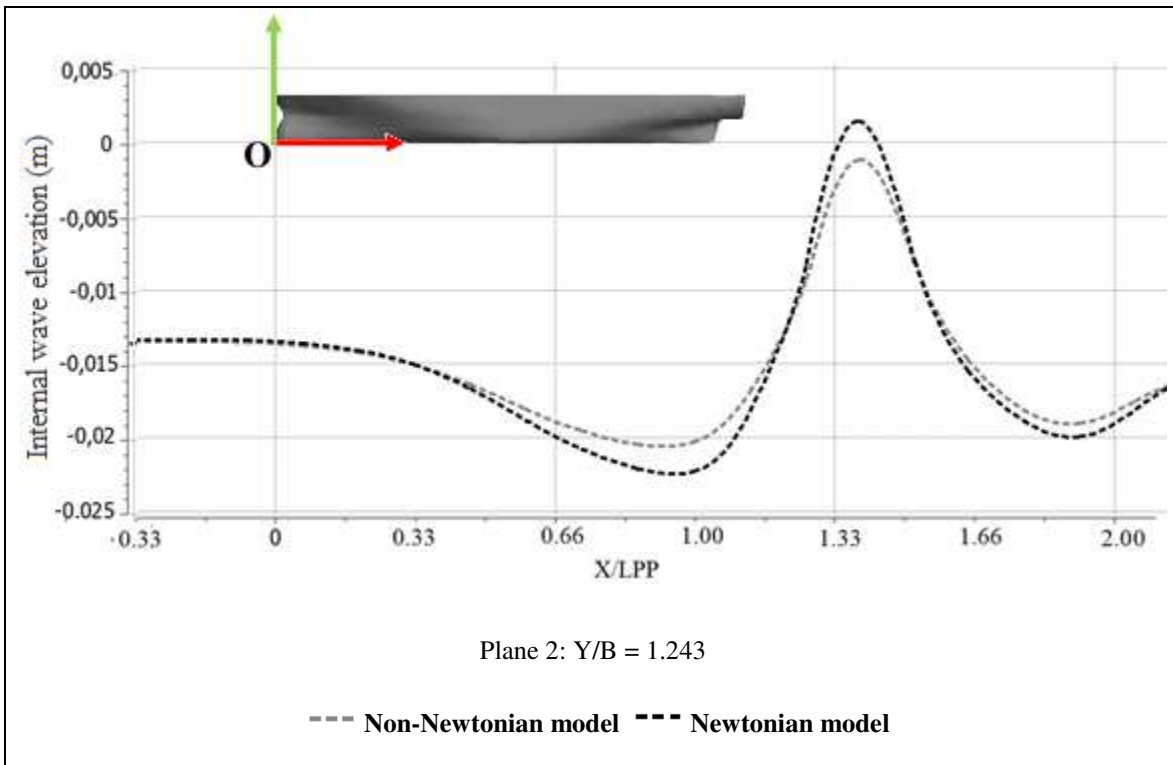
250 average thickness in the estuaries. The UKC value was set to $+10\% \cdot T$ with respect to the mud/water interface, which
251 corresponded in our case to 1 m in full scale (0.0125 m in the scaled model).

252

253 Figures 5 and 6 present a comparison between the undulations of the mud/water interface obtained using both methods
254 for mud types A and C at two different plans (see Figure 7). The first plane is located at Y/B of 0.621 while the second is
255 located at $Y/B = 1.243$, where Y is the lateral distance from the ship's mid-plan and B is the ship's beam. The x-axis of
256 these figures represented the dimensionless distance X/LPP , where X is the longitudinal distance from the ship's bow
257 and LPP is the length of the ship, and the z-axis represented the undulation elevation. Generally, we remark that the non-
258 Newtonian model tends to underestimate the mud layer crests. As is evident, the difference between both models shows
259 that mud A has a smaller viscosity and density compared to mud C. The height difference at the crest and trough is al-
260 most similar; approximately 11% at plane 1 and 18% at plane 2 for mud A, and approximately 16% at plane 1 and 30%
261 at plane 2 for mud C. The difference is larger at plane 2, because, the area affected by the ship's passage is reduced
262 when the mud is considered non-Newtonian, especially at high density and viscosity, as shown in Figure 7.

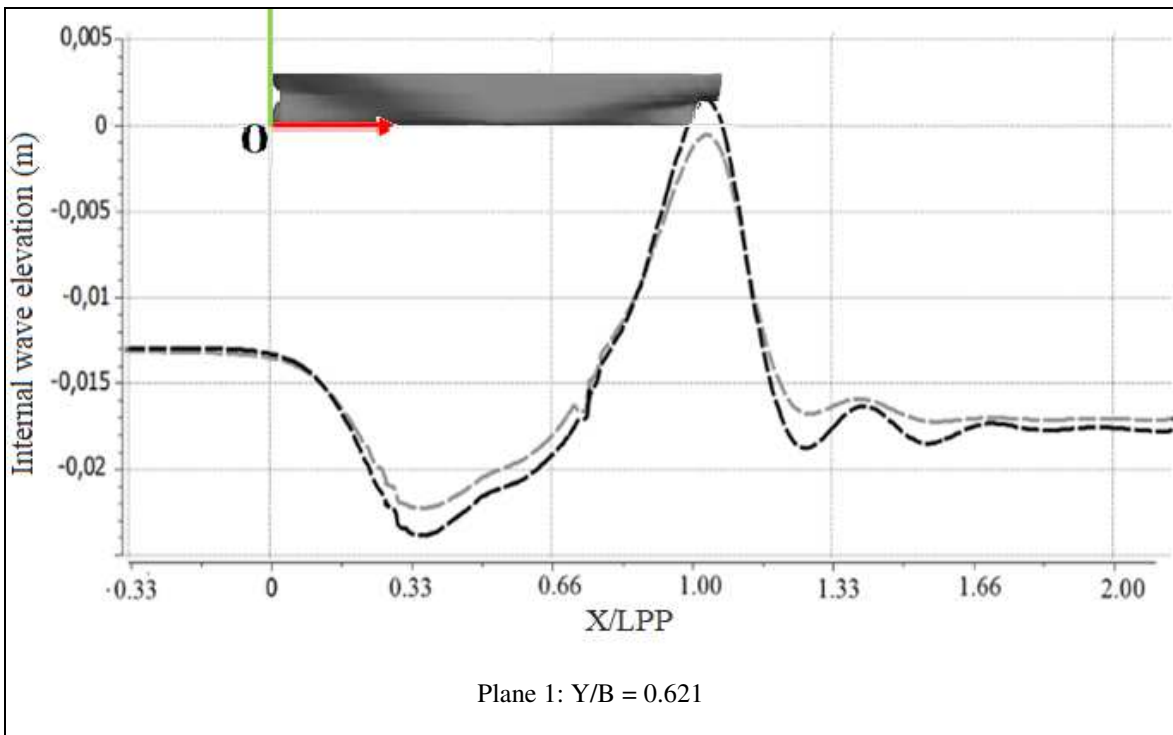
263

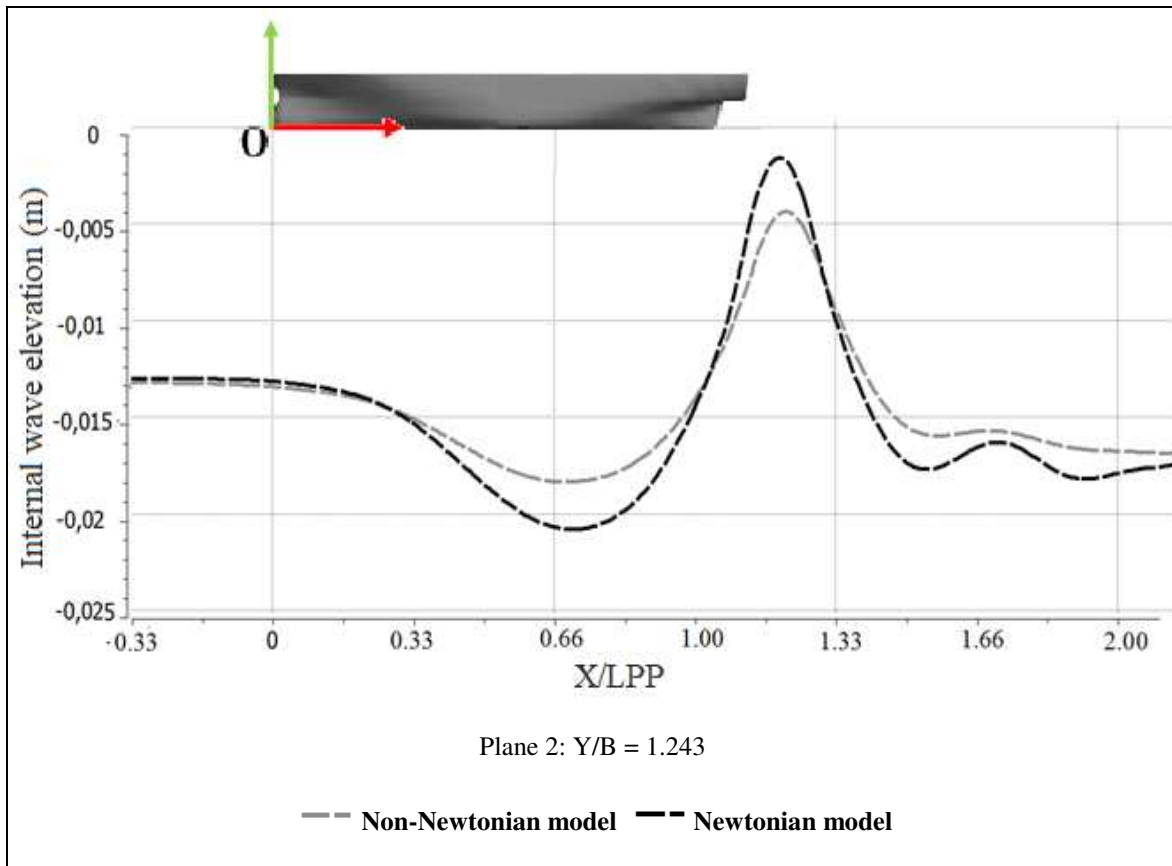




264 **Figure 5. Undulation of mud A at two different planes from the mid ship.**

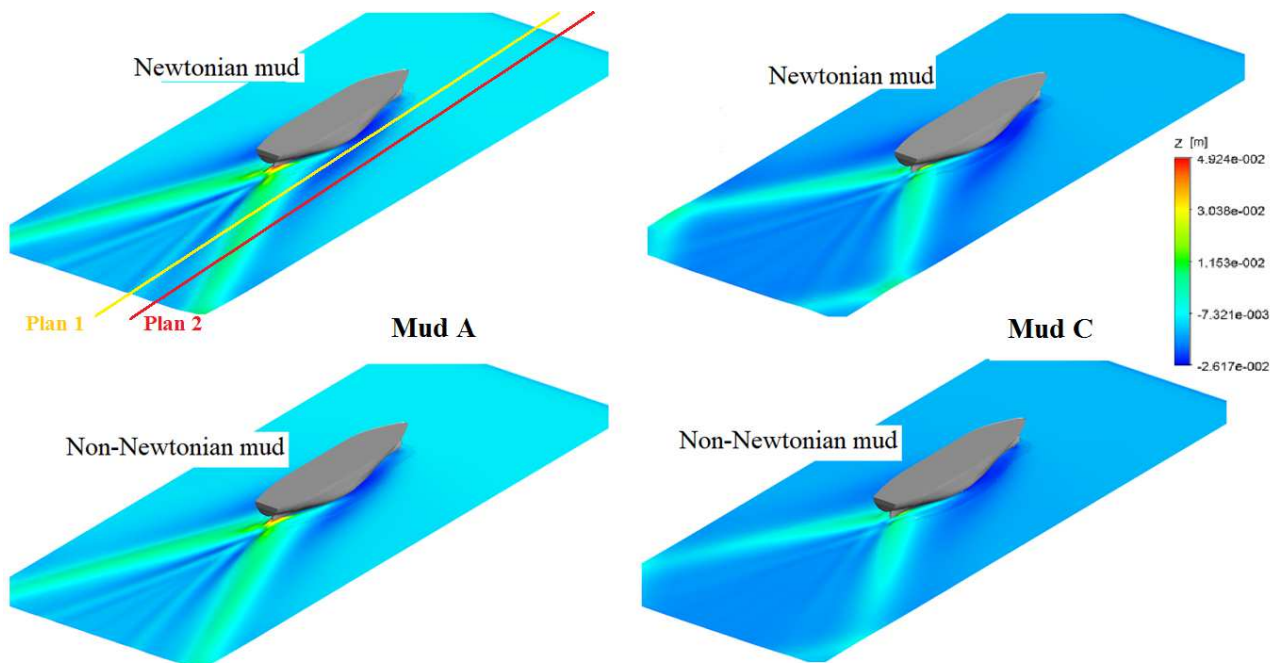
265





266 **Figure 6. Undulation of mud C at two different planes from the mid ship.**

267



268

269 **Figure 7. Iso-surface of internal waves for mud A and C by considering a Newtonian and non-Newtonian model**

270

(UKC = +10%).

271

272 To assess the ship's resistance, two UKCs were tested (+10% and -10%). For the two types of mud, the difference be-
 273 tween the Newtonian and non-Newtonian models was small, as presented in Table 3 (approximately 2% for both mud A
 274 and mud C at positive UKC, and less than 5% at negative UKC. Note that, the verification and validation procedure
 275 shows that the uncertainty of the total resistance was about 7% in very confined water. This uncertainty corresponds to a
 276 monotonic convergence condition with an order of accuracy of 1.86. Based on these values, the only conclusion that can
 277 be drawn from this comparative analysis is that the Newtonian model gives an acceptable estimation of the ship's re-
 278 sistance despite the overestimation of the mud/water undulation. Hence, the Newtonian model can be used to carry out
 279 this investigation.

280 **Table 3. Computed ship's resistance (half of ship) using the Newtonian and non-Newtonian models.**

	Ship's resistance		Δ
	Newtonian	Non-Newtonian	
UKC = +10%			
Mud A	1.125±0.078 N	1.149±0.080 N	2.08%
Mud C	1.328±0.093 N	1.356±0.095 N	2.06%
UKC = -10%			
Mud A	2.302±0.160 N	2.415±0.170 N	4.76%
Mud C	2.652±0.185 N	2.623±0.182 N	1.10%

281

282 4.2 INFLUENCE OF MUD PROPERTIES ON SEABED UNDULATION AND FREE SURFACE ATTENUA-
 283 TION

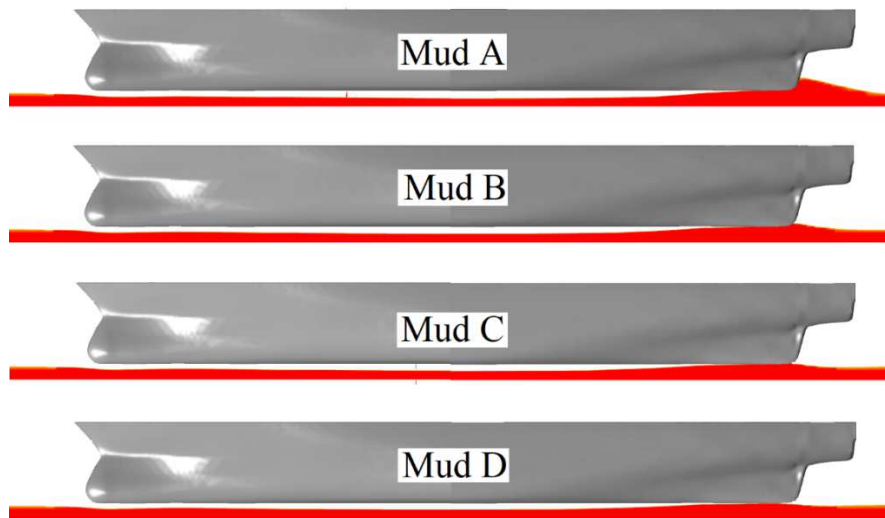
284

285 Here, the mud layer thickness was set to 3 m (0.0375 m in the scaled model). The ship's draft and speed were set to 10
 286 m (0.125 m in the scaled model) and 10 kn (0.575 m/s in the scaled model), respectively. The value chosen for the UKC
 287 with respect to the mud/water interface was +10%*T.

288

289 Figure 8 illustrates the profile of the mud layer deformation caused by the ship's passage. As can be seen, the defor-
 290 mation is composed of a principal undulation and secondary undulations. The principal undulation is similar to the free
 291 surface deformation with a small shift, where a stern divergent wave is observed (Figure 9). The divergence angle, the
 292 wave height, and the wavelength of this wave depend on the mud properties, as shown in Figure 10. In this study, we
 293 only focused on the principal undulation, which had an impact on the ship manoeuvring, principally on the ship's re-

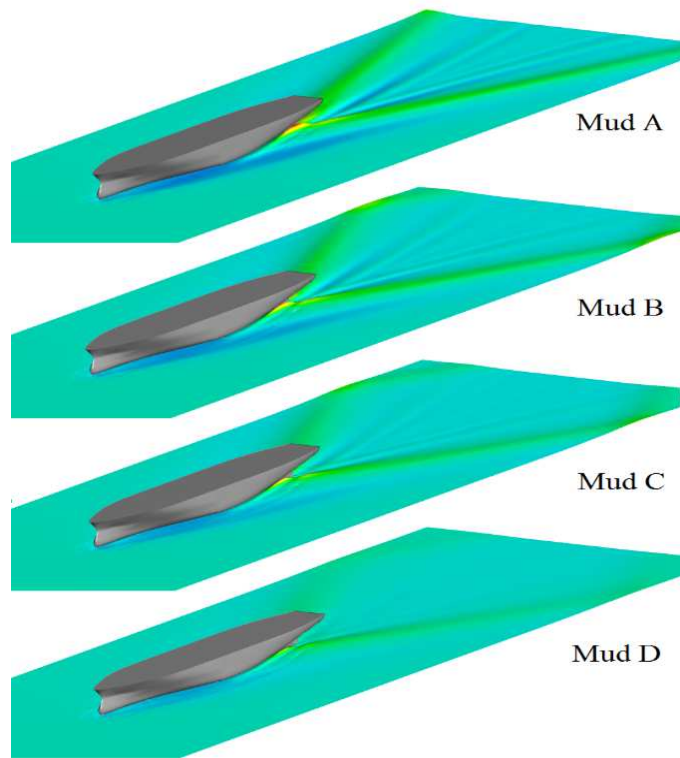
294 sistance and squat. This undulation was characterised by a maximum trough and crest, where generally the trough is
295 located at the mid hull, whilst the crest is located at the hull's stern. For all tested mud properties, the mud layer trough
296 started from the same position (the ship's bow). However, compared to the initial mud setup, the trough level and length
297 increased by decreasing the mud viscosity. We note that the origin of this trough was principally the pressure variation
298 along the ship hull caused by the return flow, which was influenced by the mud properties (see Figure 11). From the
299 same figure, it can be seen that the relative increase of the mud trough shows a linear variation for viscosities varying
300 between 0.025 and 0.12 Pa.s.



301
302 **Figure 8. Profile of the mud layer undulation at the ship symmetry plane.**

303
304 It can also be observed that the physical properties of the mud played an important role on the mud crest, the location of
305 this crest, and in some situations the hull/mud contact area. When the density and viscosity of the mud were smaller, the
306 mud was considered more fluid; hence, the later behaved as a denser fluid and followed the water flow. When the vis-
307 cosity of the mud was greater, the mud layer was more solid and its behaviour was more rigid. From this, we noted a
308 maximum uprising value for the mud D ~20% less than for mud B, whilst an insignificant variation was noted between
309 mud samples B and A.

310



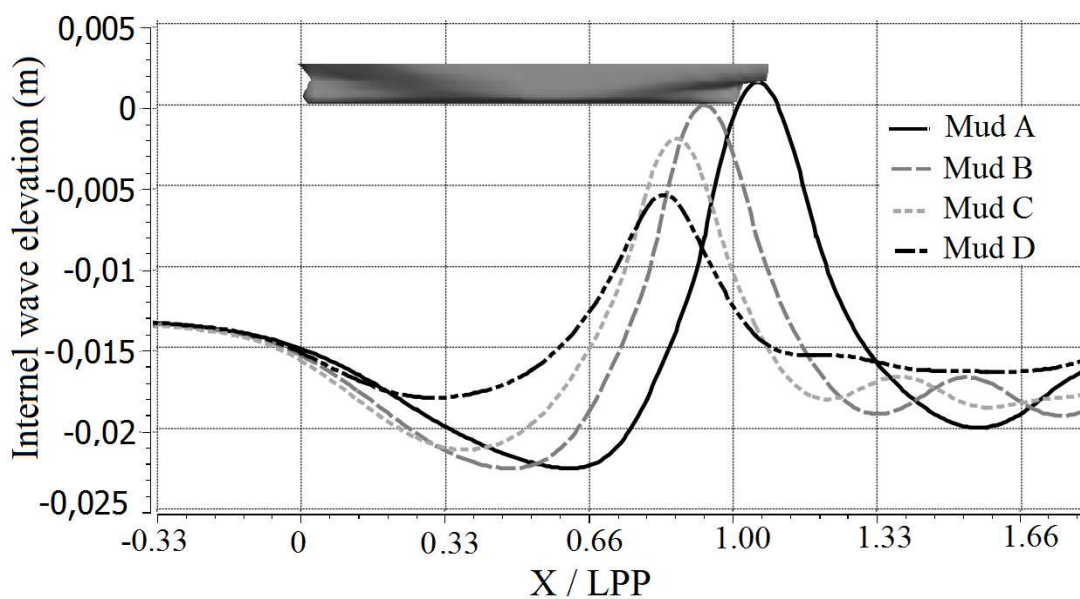
311

312

Figure 9. Iso-surface of the internal waves as a function of mud properties.

313 For all tested properties, the mud uprising position varied as the mud properties varied. From simulated cases, it was
 314 noted that the lower the viscosity, the more the mud uprising moved backwards. The same observations were also noted
 315 by Delefortrie and Vantorre (2005). Contact between the hull and the mud was also observed for mud A and B and the
 316 contact area was slightly larger in the case of mud A.

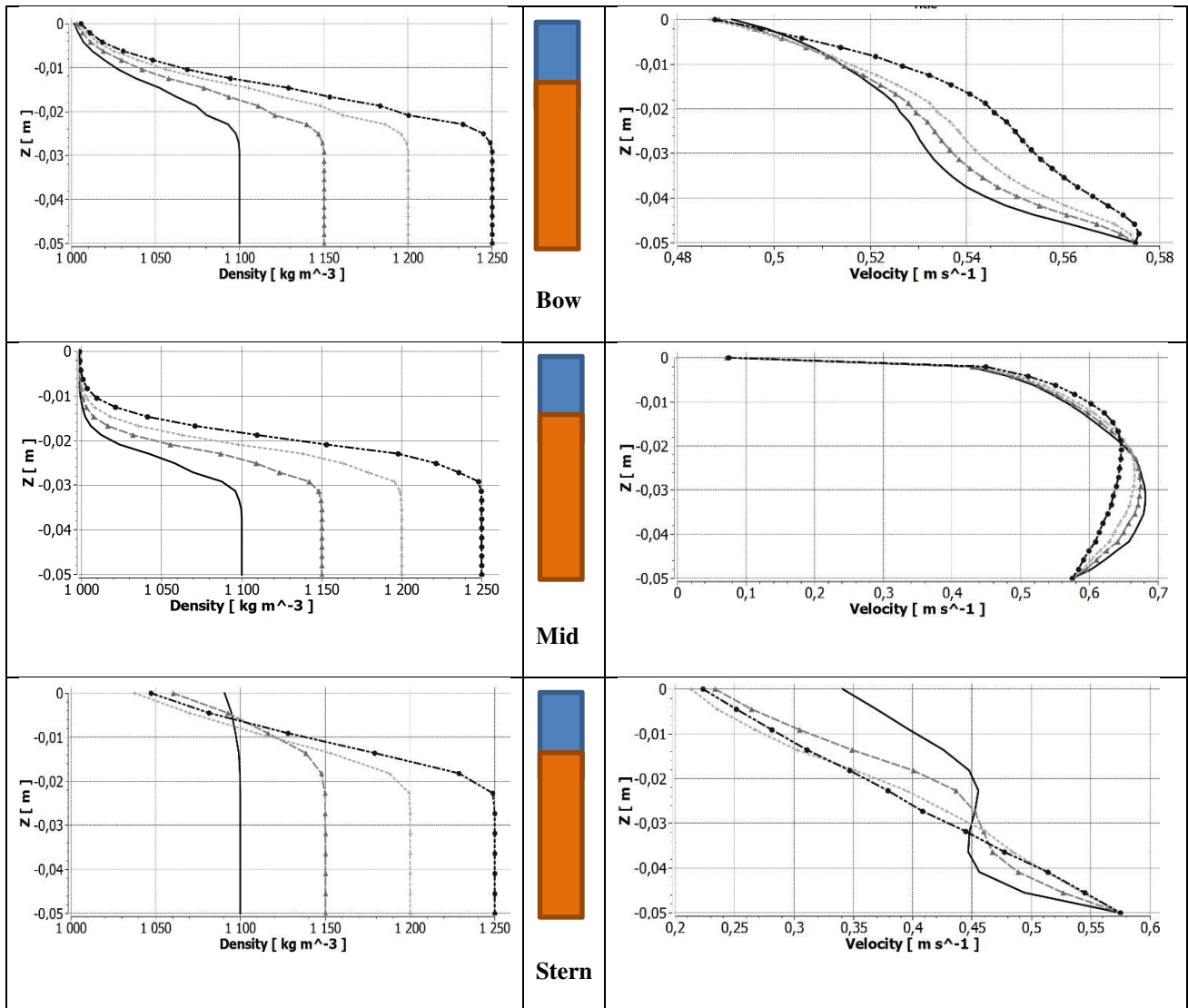
317



318

Figure 10. Mud layer undulation along the channel as a function of mud properties (cut at ship's mid-plan).

319



321 **Figure 11. Vertical profile of density and flow velocity under the ship at bow, mid, and stern of the ship.**

322

323 To assess the separate effect of the viscosity and the density on the internal waves pattern, an additional series of simula-
 324 tions were performed. For a better visibility of this undulation, the mud thickness of 3 m in full scale was used (1 m
 325 corresponds to the UKC and 2 m to the distance between the ship's keel and the solid seabed) for a negative UKC of -
 326 10%*T. Five values of viscosity and density were tested. The ship's speed was set to 10 kn as in the previous simula-
 327 tions. First, the viscosity was varied as follows: 0.005, 0.01, 0.05, 0.1, 0.2 Pa.s, while the density of the mud was set to
 328 1100 kg/m³, and second, the viscosity of the mud was set to 0.1 Pa.s which corresponds approximately to the transition
 329 limit defined by Delefortrie (2016) basing on experiments. While the density was varied as following: 1050, 1100, 1150,
 330 1200 and 1250 kg/m³.

331

332 The internal waves corresponding to the viscosity and the density variation were plotted in Figure 12. As it can be seen
333 at the left of this figure, the viscosity has a very important influence on the internal waves pattern, and for the used
334 ship's speed the internal bow waves length is longer than the ship's length which is a characteristic of shallow water
335 navigation. For the smallest viscosity, a stern waves pattern was observed, where the first is convergent, while the sec-
336 ond is divergent which resembles to the free surface behaviour in a shallow water. Reflected waves were also observed
337 far behind the ship's stern. By increasing the viscosity value to 0.01 Pa.s, the same waves pattern were observed, how-
338 ever, transverses waves appeared behind the ship's stern. For viscosity value of 0.05 Pa.s, the waves pattern becomes
339 more apparent, while the angle of the diverging waves increases and tends to be perpendicular to the ship's heading
340 direction. The same observations were noted for the viscosity value of 0.1 Pa.s, The converging waves remains un-
341 changed and apparent, whereas the diverging waves becomes completely transversal and slightly less apparent. For the
342 highest mud viscosity (0.2 Pa.s), only the transverses waves pattern were affected and becomes even less apparent and
343 tend to disappear. This behaviour, is in accordance with experimental findings, however, viscosity limits defining waves
344 patterns were slightly different.

345

346 The density variation effect on the internal waves pattern is shown at the right of Figure 12. The only observation noted
347 from this figure is that the density has any effect on the transverses waves, while the converging waves increase slowly
348 by increasing the mud density.

349

350 Basing on these results it can be concluded that the internal Froude number Fn_i ($Fn_i = Fn\sqrt{(\rho_w + \rho_m)/\Delta\rho}$) often used
351 to describe multiphasic flow cannot be used to define the internal waves patterns. It can also be concluded, that the in-
352 ternal waves pattern evolution should be set as a function of mud viscosity and mud layer thickness.

353

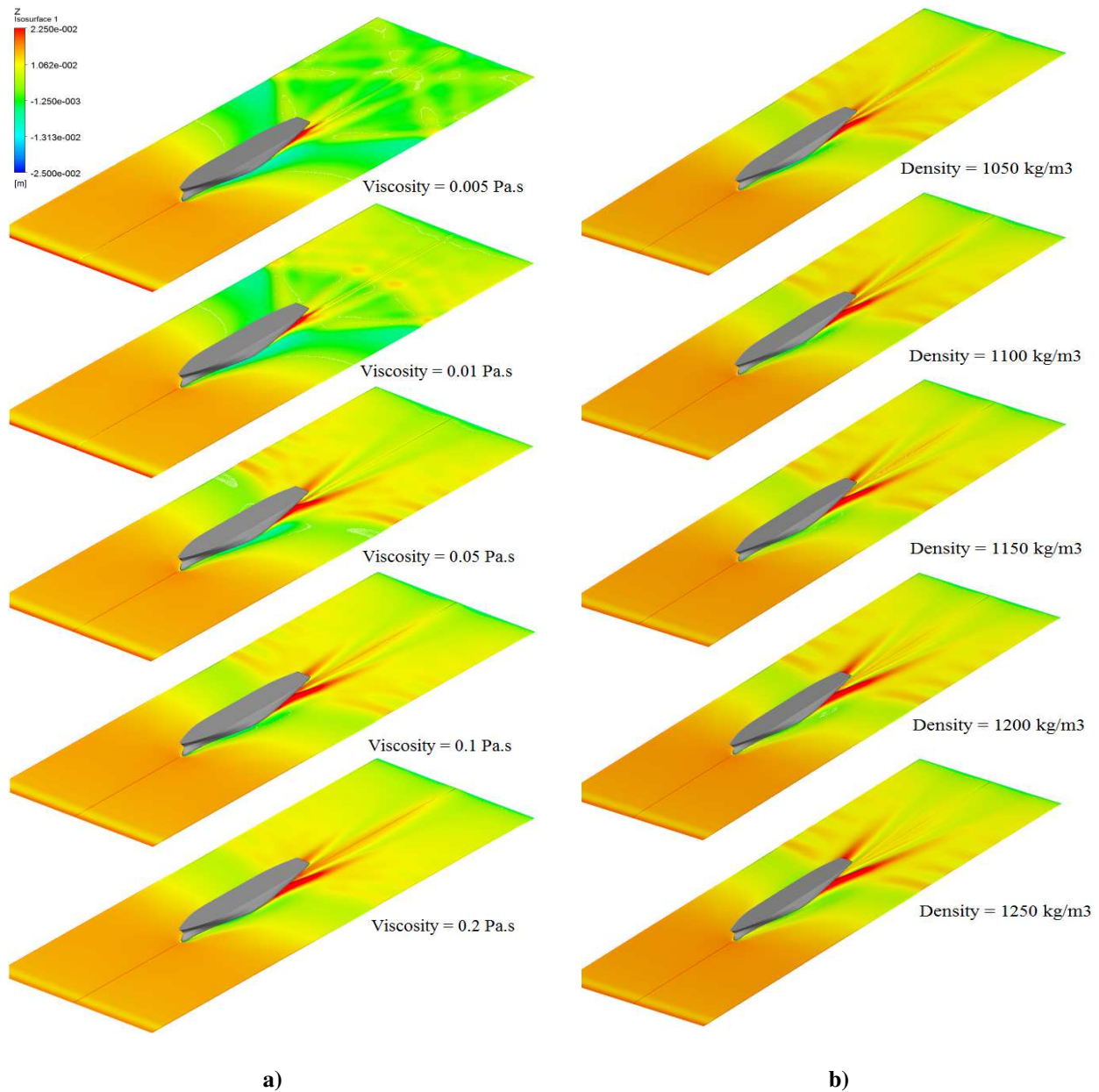


Figure 12. Internal waves: a) viscosity variation and b) density variation

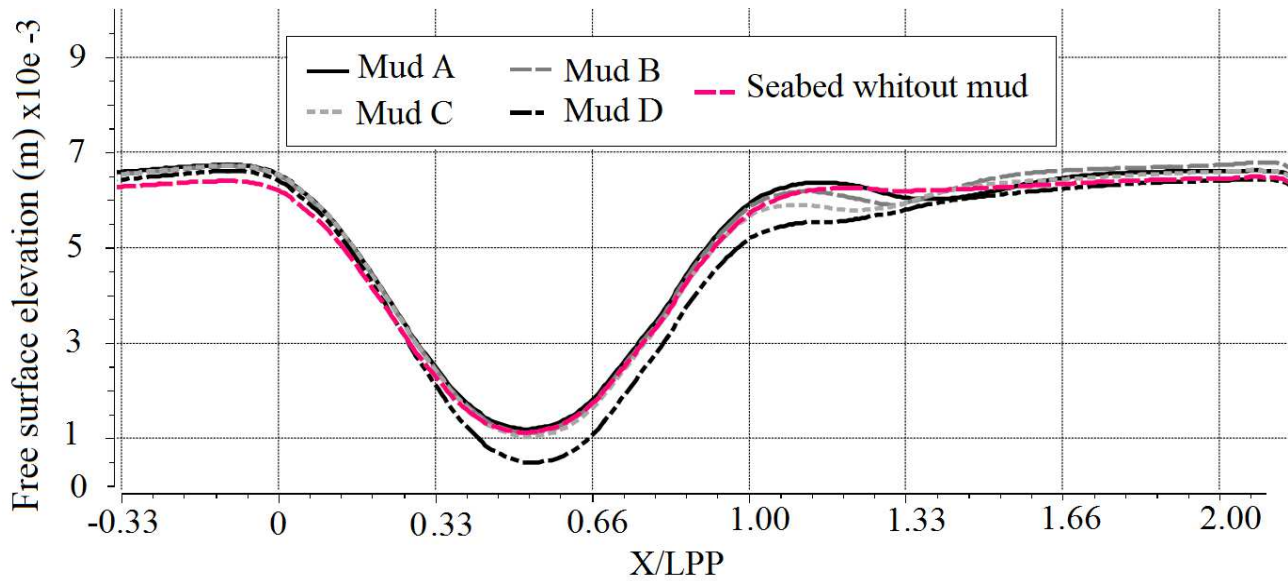
354

355

356 Figure 13 shows the free surface attenuation caused by the mud layer. For this, we compared the free surface deformation of a channel (with a muddy layer) to the free surface deformation of a channel without a muddy layer (rigid bot-
 357 tom). The same total depth was maintained for both tests. Note that for the present study, the total depth of the channel is
 358 the sum of the ship's draft, the UKC, and the mud thickness. It may be observed that the free surface elevations closely
 359 resemble the mud layer undulation. It was also observed that the trough and crest of the free surface was approximately
 360 the same between the rigid seabed and mud samples A, B, and C. However, for mud D, we noted a lowering of the free
 361 surface. This lowering was essentially caused by the effect of shallow water. As mentioned above, the higher the viscosi-
 362 ty, the more solid the mud; hence, the seabed can be considered solid. The shear stress due to the high viscosity of the
 363

364 mud slowed down the flow velocity of the mud/water interface under the ship's hull, inducing an acceleration of the
365 water flow and consequently a pressure drop.

366



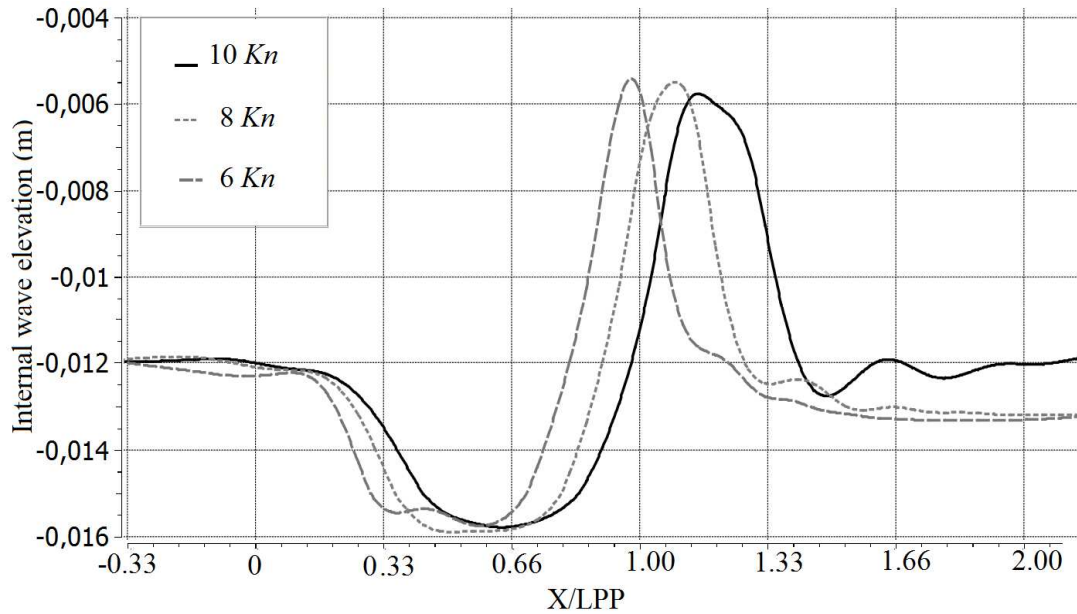
367

368 **Figure 13. Comparison between the free surface elevation of seabed with and without the muddy layer.**

369

370 4.3 SHIP'S SPEED AND MUD THICKNESS EFFECT ON THE SEABED UNDULATION (INTERNAL WAVES
371 PATTERN)

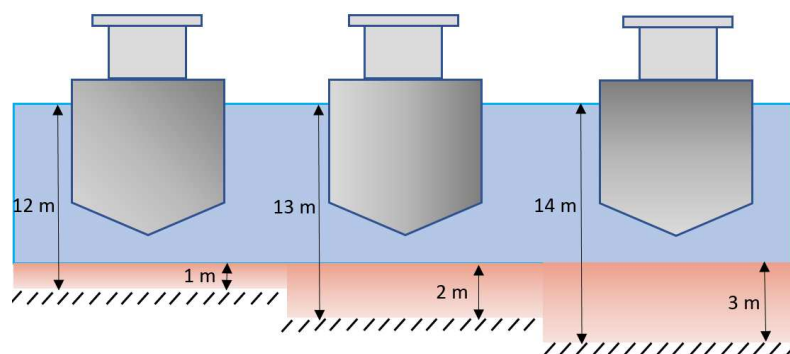
372 The study of the influence of the ship's speed and the mud's thickness on the seabed undulation is presented in this sec-
373 tion. The influence of the ship's speed was performed by setting the mud layer thickness to 3 m in full scale, and the
374 UKC to +10%*T. Mud A was selected for this simulation. The ship speeds that were tested were 6, 8, and 10 kn in full
375 scale (0.345, 0.46, and 0.575 m/s in the scaled model). It can be seen from Figure 14 that for the selected mud, the ship's
376 speed has an influence on the position of the maximum rise of the undulation. The higher the speed, the more the undu-
377 lation crest moved backwards. It was also seen that the crest width increased as the ship's speed increased. This behav-
378 iour was due first to the mud type. Here, the mud density was small and it was thus was more fluid than solid. Second,
379 the return current amplification caused by the increase in the ship's speed affected the behaviour. A slight influence of
380 the ship's speed on the trough depth and the crest height of the mud/water interface undulation was noted.



381

382 **Figure 14. Mud layer undulation along the channel as a function of the ship speed (cut at the ship's mid-plan). X**
 383 **is the longitudinal position.**

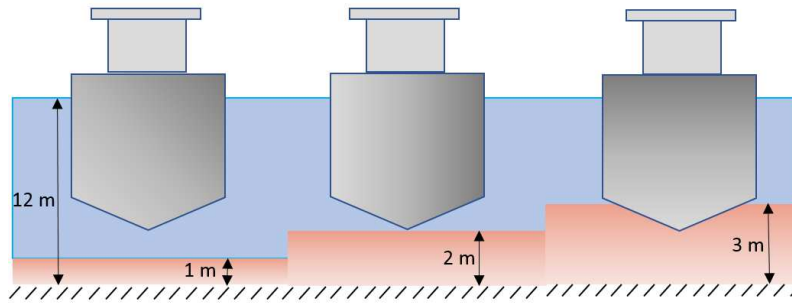
384 In the second part of this section the influence of the mud thickness on the internal waves pattern was studied. Three
 385 thicknesses of the mud A were tested: 1 m, 2 m and 3 m in full scale. Note that the mud thickness effect on the internal
 386 waves patterns can be tested using a constant UKC ($10\%*T$) and variable total depth as is depicted in Figure 15-a or
 387 using a variable UKC ($+10\%*T$, $0\%*T$ and $-10\%*T$) and constant total depth as is depicted in Figure 15-b. The ship's
 388 speed was set to 10 kn (0.575 m/s in the scaled model). The Frh values were the same for both type of test 1.64, 1.16 and
 389 0.94 (using the mud thickness as a characteristic length) for mud thickness of 1m, 2m and 3m respectively. These values
 390 correspond to critical and supercritical regimes. The numerical results of the waves patterns were shown in Figure 16.



391

392

(a)



(b)

Figure 15. Mud thickness variation: (a) variable total depth and (b) constant total depth.

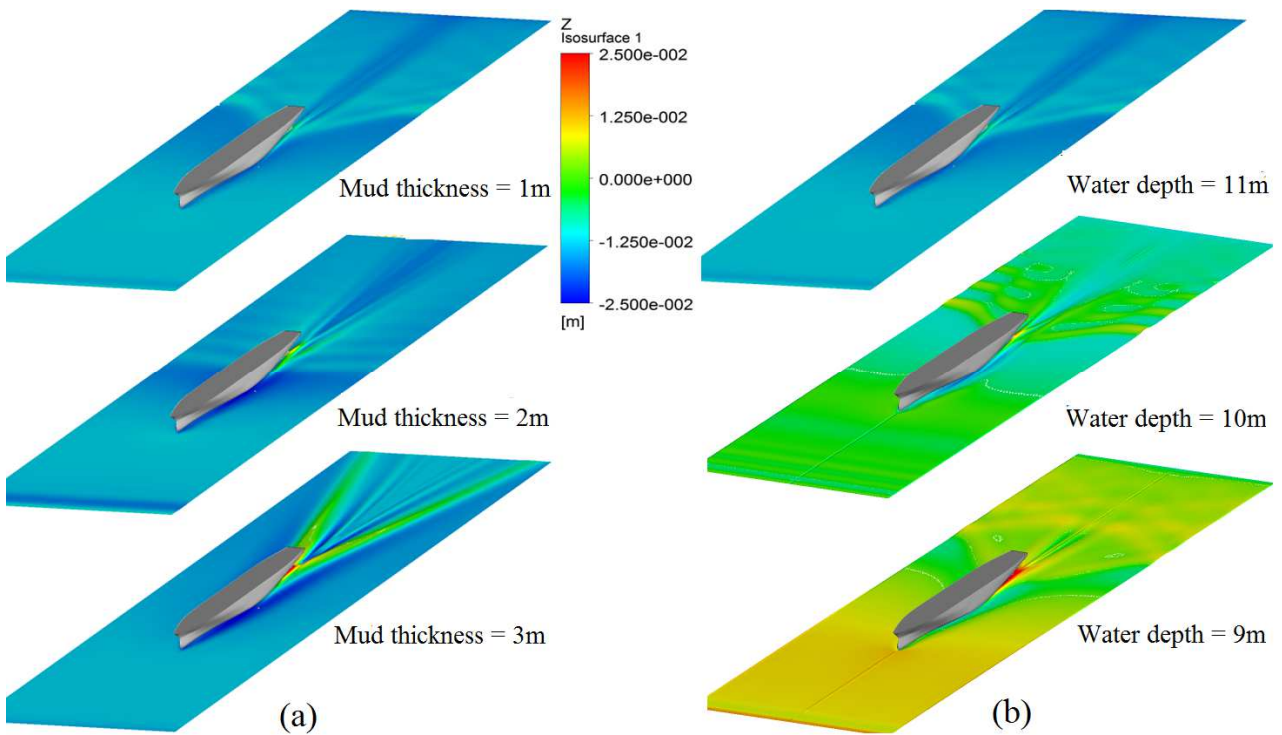


Figure 16. Internal waves patterns as a function of mud thickness : (a) constant UKC and variable total depth and (b) variable UKC and constant total depth.

Figure 16-a shows the influence of the mud thickness on the internal waves patterns for a constant UKC and variable total depth. From this figure it can be shown three different waves patterns of the seabed. Where for the smaller mud thickness (1m in full scale), the internal waves appear behind the ship's stern and its pattern is very divergent and nearly transversal to the ship's heading direction. For the medium thickness (2 m in full scale), the undulation is principally transversal, however, a small Kelvin pattern appears at the ship's stern, which leads us to consider this thickness as a transition thickness. For the larger mud thickness (3m in full scale), the internal waves have a Kelvin pattern form. These patterns were also noted in the experimental work done by Delefortrie(2016) (see Figure 17). The authors of this

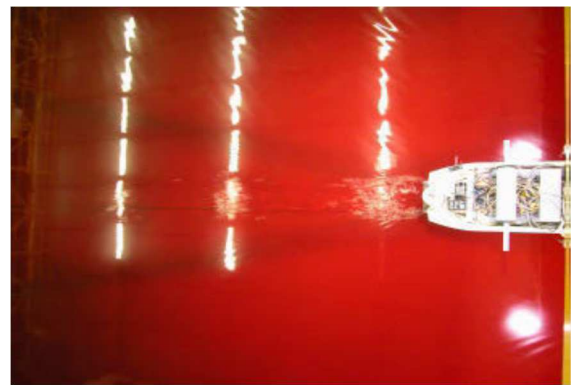
408 work related these patterns only to the mud viscosity and the ship's speed. According to their findings: the Kelvin pat-
409 tern appeared for larger ship's speed and lower viscosities ($< 0.12 \text{ Pa}\cdot\text{s}$), and the transversal pattern appeared in the case
410 of lower ship's speed. It was also noted that the transversal pattern were observed for larger ship's speed and larger mud
411 viscosities ($> 0.12 \text{ Pa}\cdot\text{s}$). In the present work the both undulation patterns (transversal and Kelvin pattern) were observed
412 by varying only the mud thickness. Where, the ship's speed can be considered larger, however, the mud viscosity is
413 lower ($0.025 \text{ Pa}\cdot\text{s}$).

414 To separate the effect of the mud thickness and the effect of the confinement, the total depth was considered constant
415 and the mud thickness was varied. The obtained results were depicted in Figure 16-b. The simulation setup for the
416 smaller mud thickness (1m in full scale) is the same as in the case of variable total depth hence the results of the previ-
417 ous simulation were kept. For the medium mud thickness (2m in full scale) the UKC is $0\%*T$, the similar waves pattern
418 as for the mud thickness of 1m was observed, however, the undulation amplitude was amplified. For larger mud thick-
419 ness ($\text{UKC} = -10\%*T$) the waves change pattern where a convergence and divergence waves appear. Transversal waves
420 were also observed far behind the ship. From these observations, it can be concluded that the mud thickness has a signif-
421 icant influence on the internal waves pattern which change as a function of the total depth and the UKC, however, it is
422 difficult to specify exactly the influence of the mud thickness. In fact, the mud thickness effect is always coupled with
423 another parameter, either the total depth or the UKC. From this study it can also be concluded that the internal waves
424 pattern are independent of the Fr_h contrary to the generated waves pattern at the water – air interface.

425
426 Basing on the results obtained in this section the pattern of internal waves are not only depends on the mud viscosity and
427 ship's speed as is given in the literature but by the combined effect of the viscosity, the ship's speed, the mud thickness,
428 the water depth and the UKC.



a) $\eta = 0.002 \text{ Pa}\cdot\text{s}$



b) $\eta = 0.030 \text{ Pa}\cdot\text{s}$

Figure 17. Measured mud layer undulation carried out by Delefortrie (2016)

429

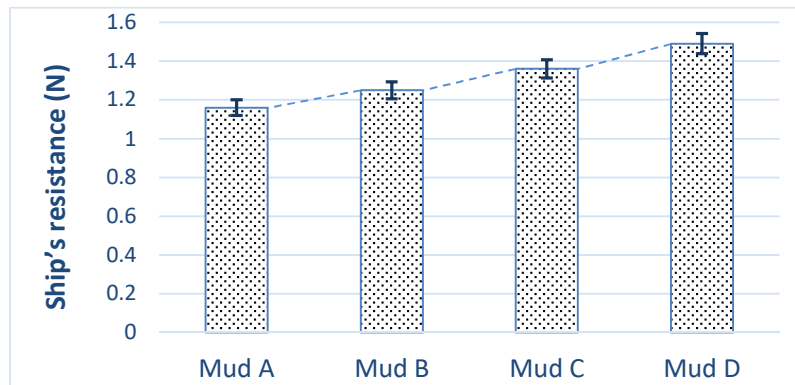
430

431 4.4 SHIP'S RESISTANCE VARIATION DUE TO MUD PROPERTIES, SHIP'S SPEED AND MUD THICKNESS

432 It is known that ship's resistance is greatly affected by channel configuration (such as confinement and restrictions). In
433 shallow water, the ship's resistance increases significantly due to the accelerated water around the hull, as explained
434 previously. The presence of the mud layer in turn affects the flow under the ship's hull, inducing a variation in the ship's
435 resistance. The effect of the latter can be considerably amplified if the UKC is negative.

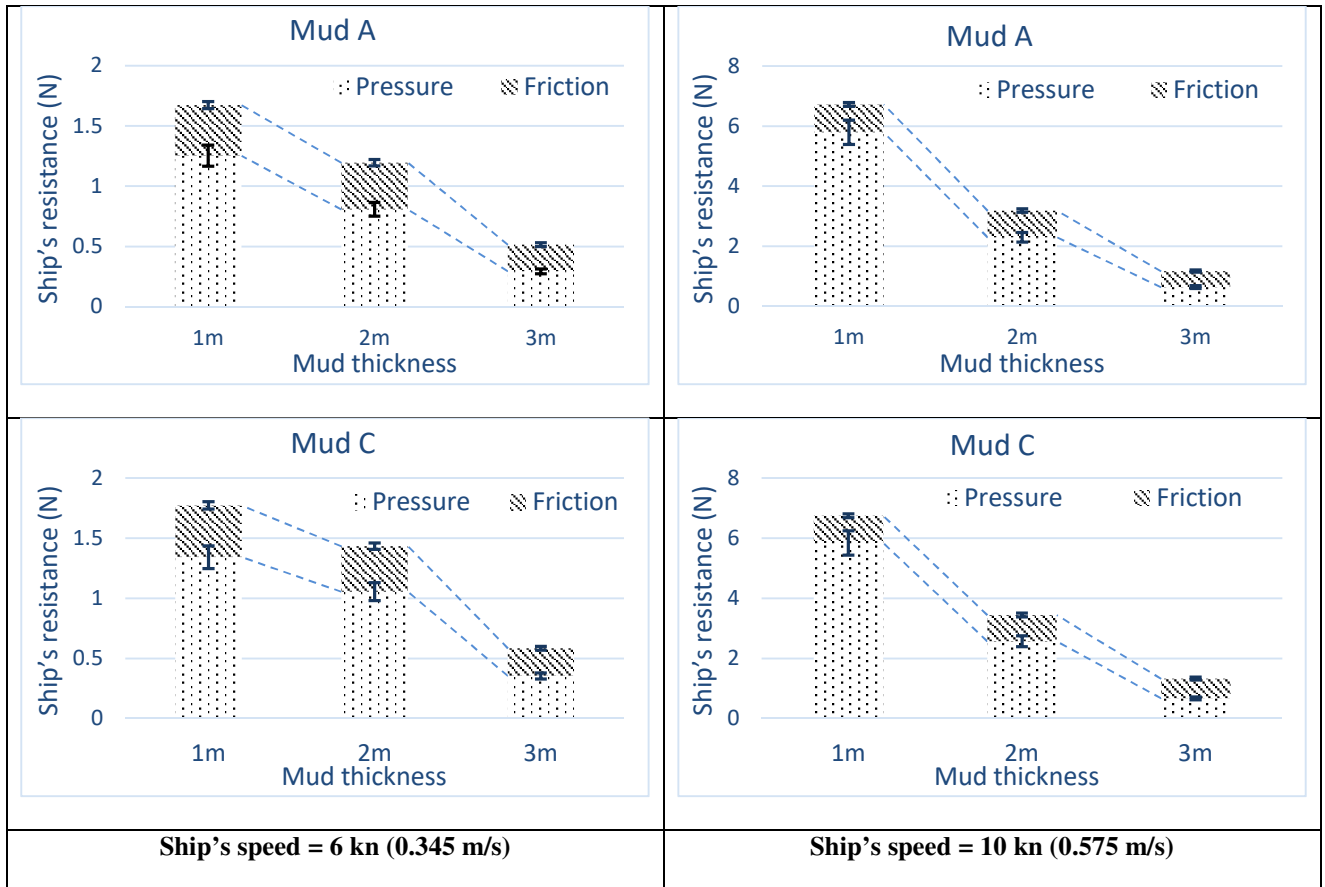
436
437 In this section, findings are presented from studying the impact of the mud layer, first by testing the mud properties
438 effect for a given mud thickness (3 m in full scale). Hence, the four mud properties were tested for an UKC of $+10\%*T$
439 with respect to the mud/water interface. The ship's speed was set to 10 kn (0.575 m/s). No squat was considered in these
440 simulations.

441
442 Figure 18 shows the ship's resistance variation caused by variations in the mud properties. From this figure, it is evident
443 that the ship's resistance increased with mud viscosity, although there was no contact between the hull and the mud with
444 mud samples C and D. This leads us to conclude that this increase essentially concerns the frictional component of the
445 resistance. In fact, when the mud is consolidated it seems as though the total depth of the water is reduced, which makes
446 the navigation environment more confined, and consequently, the return current velocity increases.



447
448 **Figure 18. Ship's resistance (half of ship) as a function of mud properties (for a ship speed of 10 kn and UKC of**
449 **$+10\%*T$).**

450
451 To understand better the confinement phenomenon due to the mud layer and its influence on the ship's resistance, we
452 carried out simulations by varying the mud thickness. Three thicknesses were tested (1m, 2m and 3m in full scale). For
453 each thickness we used two speeds (6 and 10 kn) and two types of mud (mud A and mud C). The water depth remains
454 unchanged for all simulations (10 m in full scale). First, a positive UKC of $+10\%*T$ was considered. The results of
455 these simulations were shown in Figure 19.



457
458
459
460

Figure 19. Ship's resistance (half of ship) variation as a function of mud thickness and ship's speed for mud A and mud C. UKC = +10%*T.

461 From these figures, it can be seen that the ship's resistance increases with increasing ship's speed. However, this in-
462 crease is different according to the mud layer thickness as well as the type of the mud. In fact, by decreasing the mud
463 layer thickness, the ship's resistance increases considerably. This increase concerns both types of forces: pressure and
464 friction, however, the wave-making resistance remains the most dominant and the most impacted by this decrease in
465 thickness.

466 The wave-making resistance is amplified about 9 times when the ship is sailing at a speed of 10 kn on a mud thickness
467 of 1 m than 3 m, and about 4 times when the ship's speed is 6 kn. While the amplification of the friction resistance is of
468 the order of 2 times for the two ship's speeds. It was also observed that the wave-making resistance was the most domi-
469 nant compared to the friction resistance except in the case of the largest thickness (3 m), where both types of forces were
470 approximately in the same range. This leads us to conclude that

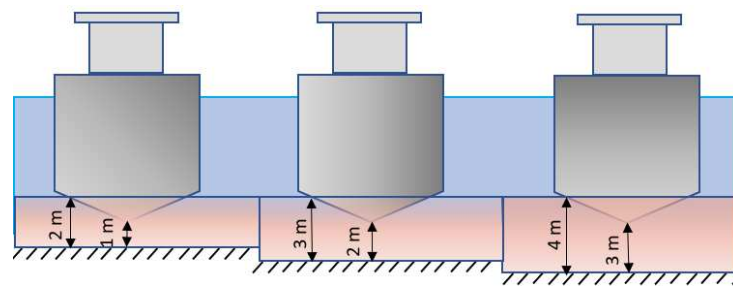
471

472 Note that for navigation in channels with solid seabed the confinement is often defined by the ratio of water depth to
473 ship's draft (hw/T). This ratio is an essential element for the calculation of the ship's resistance. In the case of navigation

474 in turbid water with a muddy bottom, this ratio may be valid however, the definition of the depth h_w must be modified
475 by including the thickness of the mud layer. A proposal has already been made by Delefortrie (2016) proposing the use
476 of the hydraulic depth (h^*) given by the following formula:

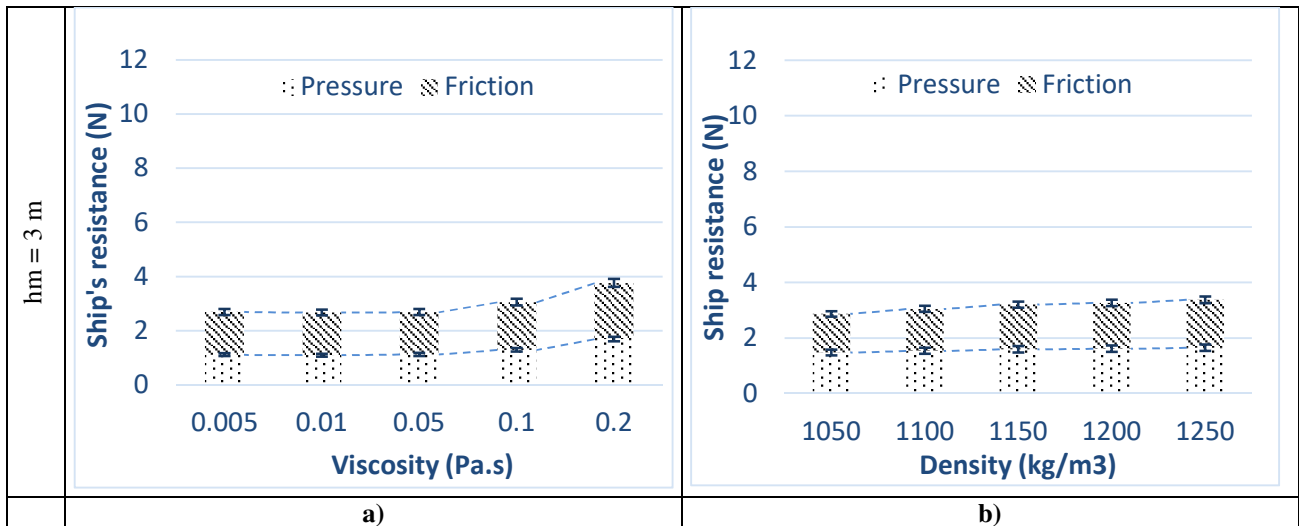
$$477 \quad h^* = h_w + \varnothing h_m \quad (11)$$

478 Where, \varnothing is the fluidization parameter which represents the mud type. So far, all works studying the influence of the
479 mud quality on the ship's resistance were performed by varying both values of viscosity and density. In order to distin-
480 guish the influence of each physical property we varied separately the viscosity and the density of the mud. The same
481 process as in the sub-section 4.3 was used: first, the density is fixed at 1100 kg / m and the viscosity is varied, then the
482 viscosity is fixed at 0.1 Pa.s and the density is varied. For a better presentation of the influence of these properties on the
483 ship's resistance, we considered the highest speed of navigation (10 kn) and assume that the ship's UKC is $-10\% * T$.
484 Three mud layer thicknesses were tested (2 m, 3 m and 4 m) corresponding to a distance between the ship's keel and the
485 solid seabed of 1 m, 2 m and 3 m as is presented in Figure 20.



486
487 **Figure 20. Mud thickness variation for an UKC value of $-10\% * T$.**

488
489 The computed ship's resistances as a function of the mud viscosity and density were presented in Figure 21 by its two
490 components: wave-making and friction. Basing on these results it was noted that for smaller and medium mud thick-
491 nesses the wave-making resistance is dominant compared to the friction resistance, however, for the larger mud thick-
492 nesses, the friction resistance is dominant. This behavior is physical, because it depends on the depth Froude number.
493 Where for high values of depth Froude number the wave-making resistance is dominant while the friction resistance is
494 dominant for very lower values. By analyzing the numerical results of the ship's resistance under the variation of the
495 viscosity, it can be seen that the effect of the later begins to be visible when the viscosity is more than 0.01 Pa.s in small-
496 er and medium mud thicknesses. For the larger mud thickness the effect is visible only when the viscosity of the mud is
497 greater than 0.05 Pa.s. It can also be seen that despite the dominance of the wave-making resistance, its variation at a
498 given mud thickness is insignificant compared to the variation of the friction resistance. Where, the maximum variation
499 of the wave-making resistance is about 30% computed between the largest and the smallest value of the viscosity at the



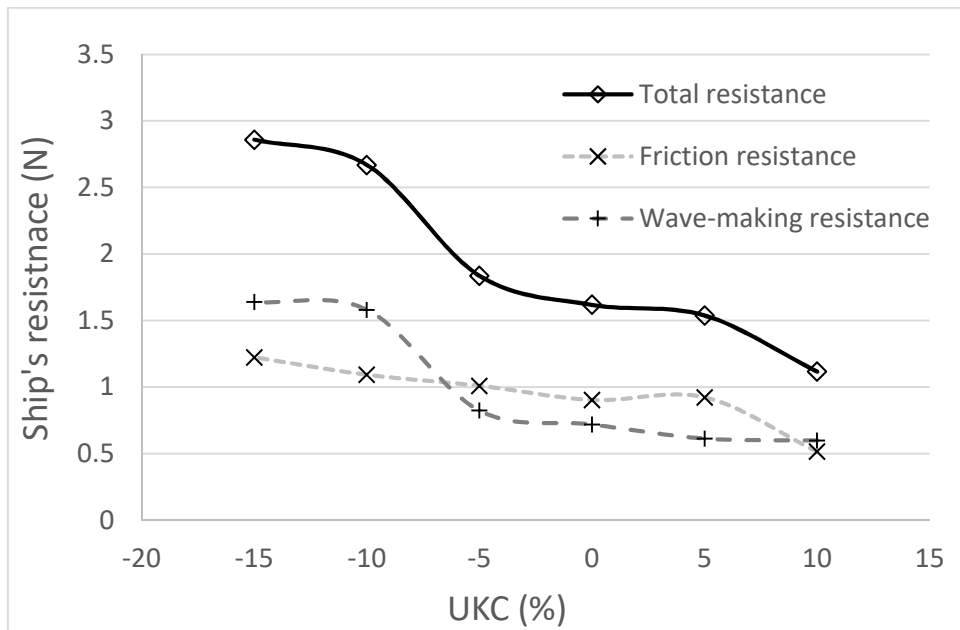
512 **Figure 21. Ship's resistance variation (half of ship) as a function of mud thickness: a) viscosity variation and b)**
 513 **density variation**

514
 515 The second part of this section presents the results for the ship's resistance, studied as a function of the UKC. Mud A
 516 was used for 6 values of UKC, as follows: +10%, +5%, 0%, -5 %, -10%, and -15% of the ship's draft. The ship's draft
 517 here was 10 m, the mud thickness was 3 m, and the speed of the ship was 10 kn.

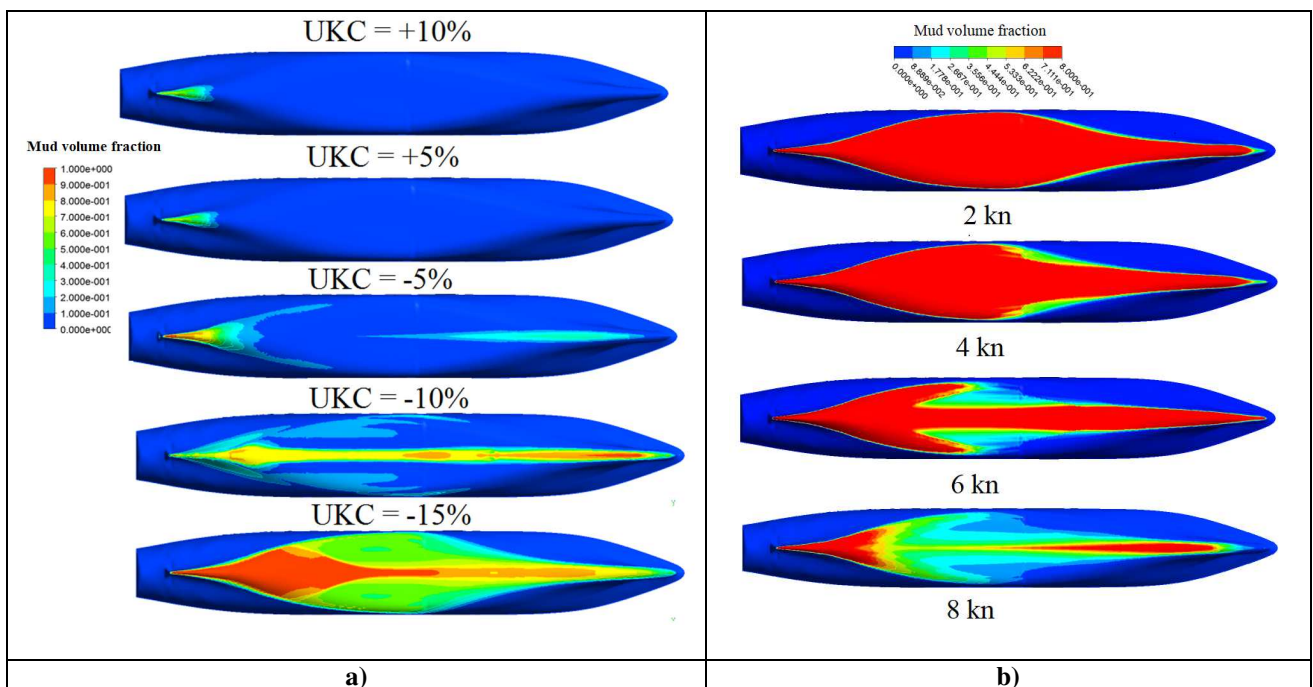
518
 519 From Figure 22, we observe an increase of the total resistance with the decrease of the UKC. The pressure resistance
 520 dominates for UKC, varying between +10 and -5%*T. Less than that, the frictional force dominates considerably. We
 521 also observe that ship's resistance increase is very slight for UKC values between +5% and -5% and less than -10%. The
 522 ship's resistance increase is significant only between +10% and +5%, and between -5% and -10%. By analysing Figure
 523 23-a plotting the area of contact between the hull and the mud, we note that for UKC range of +10%–+5%, the contact
 524 area is almost the same and the total resistance increase is principally due to the shallow water effect. For the UKC range
 525 -5%---10%, the resistance increase is principally due to the hull/mud contact. As is shown in Figure 22, the frictional
 526 resistance dominates while the pressure resistance increases slightly.

527
 528 It can also be observed from Figure 23-a that when the ship is sailing inside the mud layer (negative UKC); the keel of
 529 the hull is not fully covered by the mud. This is one of the relevant phenomena observed in this work. In fact, when the
 530 ship is sailing in the mud, we observe two different behaviours. When the ship's speed is low, the ship's keel is fully
 531 covered by the mud. However, when the ship's speed increases, the top boundary of the mud layer tends to be more
 532 liquefied, especially at the ship's bow, and a film of very liquefied mud (or turbid water) is created between the mud and

533 the hull. Figure 23-b, shows the evolution of the hull-mud contact area as a function of the ship's speed (to illustrate
 534 bitter the contact area, the legend of this figure was limited to a volume of fraction of 0.8)



535
 536 **Figure 22. Ship's resistance (half of ship) as a function of UKC (mud A).**
 537



538 **Figure 23. Hull-Mud contact area (mud A): a) as a function of UKC and b) as a function of ship's speed for an**
 539 **UKC of -10%.**

540 4.5 EFFECT OF THE MUDDY SEABED ON THE SHIP'S SQUAT

541 One of the aims of this work was the numerical study of the influence of the muddy layer on the ship's squat (sinkage
 542 and trim). The fluid-structure interaction is treated by a modified Newton algorithm coupled to a steady RANS (Linde et

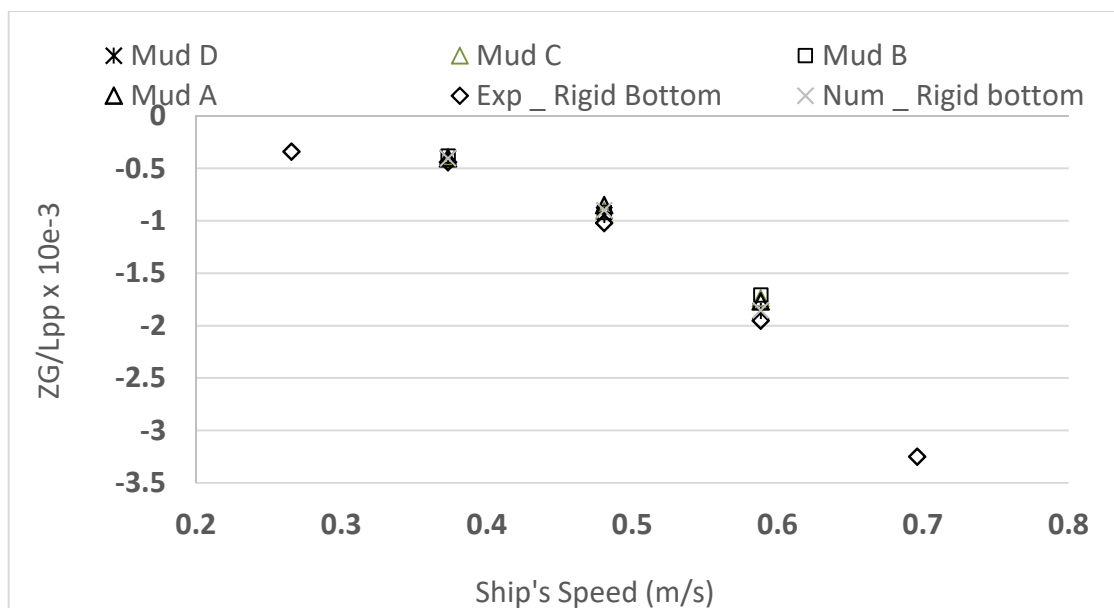
543 al., 2016). The standard dynamic Newton algorithm was not used because of several numerical complications encoun-
544 tered. The origin of these complications is essentially the bad estimation of the added mass due to the high blockage
545 coefficient, which considerably affects the stability and convergence of the numerical solution.

546
547 Because of the large computation time, only one mud layer thickness was considered (2 m) for an UKC of +10%*T. The
548 effect of the mud properties on the squat was simulated for the four types of mud and for three ship speeds (6, 8, and 10
549 kn), which correspond to a Froude depth number (Fr_h) of 0.297, 0.396, and 0.495, respectively.

550
551 The ship's sinkage as a function of the mud type was plotted in Figure 24 and compared to the experimental and numeri-
552 cal sinkage for a rigid bottom.

553
554 Concerning the ship's sinkage, similar observations given by Delefortrie (2016) were noted. First, we observed that the
555 sinkage obtained numerically for a rigid seabed was in accordance with measurements. We also observed that the sink-
556 age increased by increasing the ship's speed in all configurations with or without the mud layer. However, the sinkage
557 values decreased slightly with the change in mud properties. For larger viscosities (Mud C and Mud D), we observed an
558 insignificant decrease, whilst a moderate decrease was observed for Mud A and Mud B. This decrease augmented in turn
559 with the increase in the ship's speed. In fact, this increase was due to the added buoyancy generated by the contact be-
560 tween the hull and the mud. This contact, as mentioned previously, was located at the ship's stern when the undulation
561 crest was larger, as for Mud A and Mud B.

562



563

564 **Figure 24. Ship sinkage as a function of the mud properties for an UKC of +10%. Z_G is the sinkage at the mid**
 565 **ship**

566
 567 The ship's trim was plotted in Figure 25. For the selected UKC, the trim has positive values, which correspond to a trim
 568 by the stern. The plotted results show that the numerical results are in the same range as measurements without mud. It
 569 can also be seen that the mud had an insignificant effect on the trim at low ship speed (6 kn) in the case of Mud B, C,
 570 and D. Except in the case of the Mud A, a significant deviation compared to the rigid bottom case was observed. For a
 571 ship speed of 10 kn, this deviation decreased, due to the mud-hull contact located at the stern of the ship, which created
 572 an asymmetry in the ship's buoyancy. However, the trim behaved differently in the case of Mud D, where the trim de-
 573 viation (compared to the rigid bottom case) increased with the ship's speed. This increase can be explained by the con-
 574 finement that this type of mud generates.

575
 576 Note that some of these observations are not in agreement with observations made by Delefortrie (2016), based on
 577 measurements carried out in the towing tank for Manoeuvres in Confined Water at Flanders Hydraulics Research, Ant-
 578 werp (in Co-operation with Ghent University).



579
 580 **Figure 25. Ship trim as a function of the mud properties for an UKC of +10%.**

581
 582
 583
 584
 585

586 **5 CONCLUSIONS**

587 In this paper, an overview of a numerical investigations on the impact of muddy seabed on a ship's resistance and squat
588 was presented. A multi-phase CFD model was used to estimate the ship's resistance and squat as a function of several
589 parameters: different configurations.

590 Based on observations noted in the present work, it was concluded the following:

- 591 • The obtained numerical results are in agreement with physical models results;
- 592 • The internal waves crests depend strongly on the mud properties;
- 593 • The internal waves patterns depend strongly on several parameters: the viscosity, the total depth, the UKC and
594 the thickness of the mud layer and the Frh is not adapted to characterize the waves pattern.
- 595 • The internal waves influence the ship's resistance and squat especially when the UKC is negative;
- 596 • The effect of the mud layer on the ship's sinkage is significant only when the UKC is negative;
- 597 • The effect of the mud on the ship's resistance can be felt even when the UKC is positive, and this depends on
598 the mud properties;
- 599 • The ship's speed tends to move the mud/water interface undulation in the backwards.

600 The ability of the CFD method to simulate multiphase flow and interaction between the fluid flow and the structure has
601 been demonstrated. Some difficulties were encountered in the modelling of the depth-dependent density and viscosity of
602 the mud. Some difficulties were also encountered in the simulation of the dynamic ship squat, especially when the mud
603 contacted the ship's hull. An improvement can be made in future works by integrating a new numerical algorithm that
604 stabilises calculations and takes into account the real vertical profile of the density.

605

606 **6 ACKNOWLEDGEMENTS**

607

608 The work presented in this paper was performed within the project "Gironde-XL" funded by "Le Grand Port Maritime
609 de Bordeaux" and the European commission.

610

611 **7 REFERENCES**

612

613 AlChang, Y., Zhao, F., Zhang, J., Hong, F.-W., Li, P., Yun, J., 2006. Numerical simulation of internal waves excited by
614 a submarine moving in the two-layer stratified fluid. *J. Hydrodyn. Ser. B* 18, 330–336.

615 Crapper, G.D., 1967. Ship waves in a stratified ocean. *J. Fluid Mech.* 29, 667–672.

616 Debaillon, P., 2010. Numerical investigation to predict ship squat. *J. Sh. Res.* 54, 133–140.

617 Delefortrie, G., 2016. Ship Manoeuvring Behaviour in Muddy Navigation Areas, in: *Proceedings of 4th MASSHCON*.
618 pp. 26–36. <https://doi.org/10.18451/978-3-939230-38-0>

619 Delefortrie, G., Vantorre, M., 2005. Modelling navigation in muddy areas, *Hydronav'05 - Manoeuvring '05: Joint 16th*
620 *International Conference on Hydrodynamics in Ship Design and 3rd International Symposium on Ship*
621 *Manoeuvring*, Ostróda, Poland, September 2005.

622 Delefortrie, G., Vantorre, M., Eloot, K., 2004. Linear manoeuvring derivatives in muddy navigation areas. *Trans. R.*
623 *Inst. Nav. Archit. Int. J. Marit. Eng.* 146, 1–13.

624 Eloot, K., Delefortrie, G., Vantorre, M., Quadvlieg, F., 2015. Validation of ship manoeuvring in shallow water through
625 free-running tests, in: *Proceedings of the ASME 2015 34th International Conference on Ocean, Offshore and*
626 *Arctic Engineering*.

627 Esmailpour, M., Martin, J.E., Carrica, P.M., 2016. Near-field flow of submarines and ships advancing in a stable
628 stratified fluid. *Ocean Eng.* 123, 75–95.

629 Gourlay, T., 2008. Slender-body methods for predicting ship squat. *Ocean Eng.* 35, 191–200.

630 Hudimac, A.A., 1961. Ship waves in a stratified ocean. *J. Fluid Mech.* 11, 229–243.

631 ITTC, 2011. *ITTC – Recommended Procedures and Guidelines - Verification and validation of linear and weakly*
632 *nonlinear seakeeping computer codes. 7.5-02-07-02.5 (Revision 01)* 17.

633 Kaidi, S., Smaoui, H., Sergent, P., Daly, F., 2018. Numerical investigation of the impact of the inland transport on bed
634 erosion and transport of suspended sediment : propulsive system and confinement effect. *PIANC-World Congress,*
635 *Panama*, pp. 0–12.

636 Kaidi, S., Smaoui, H., Sergent, P., 2018. CFD Investigation of Mutual Interaction between Hull , Propellers , and
637 Rudders for an Inland Container Ship in Deep , Very Deep , Shallow , and Very Shallow Waters. *J. Waterw. Port,*
638 *Coastal, Ocean Eng.* 144. [https://doi.org/10.1061/\(ASCE\)WW.1943-5460.0000458](https://doi.org/10.1061/(ASCE)WW.1943-5460.0000458).

639 Kaidi, S., Smaoui, H., Sergent, P., 2017. Numerical estimation of bank-propeller-hull interaction effect on ship
640 manoeuvring using CFD method. *J. Hydrodyn.* 29. [https://doi.org/10.1016/S1001-6058\(16\)60727-8](https://doi.org/10.1016/S1001-6058(16)60727-8)

641 Linde, F., Ouahsine, A., Huybrechts, N., Sergent, P., 2016. Three-dimensional numerical simulation of ship resistance in
642 restricted waterways: Effect of ship sinkage and channel restriction. *J. Waterw. Port, Coastal, Ocean Eng.*
643 6016003.

644 Ma, C., Zhang, C., Chen, X., Jiang, Y., Noblesse, F., 2016. Practical estimation of sinkage and trim for common generic
645 monohull ships. *Ocean Eng.* 126, 203–216.

- 646 Mucha, P., el Moctar, O., Böttner, C.-U., 2014. Technical Note: PreSquat – Workshop on Numerical Prediction of Ship
647 Squat in Restricted Waters. *Sh. Technol. Res.* 61, 162–165.
- 648 Razgallah, I., Kaidi, S., Smaoui, H., Sergent, P., 2018. The impact of free surface modelling on hydrodynamic forces for
649 ship navigating in inland waterways: water depth, drift angle, and ship speed effect. *J. Mar. Sci. Technol.*
650 <https://doi.org/10.1007/s00773-018-0566-y>
- 651 Sergent, P., Lefrançois, E., Mohamad, N., 2015. Virtual bottom for ships sailing in restricted waterways (unsteady
652 squat). *Ocean Eng.* 110, 205–214.
- 653 Stern, F., 2013. Computational ship hydrodynamics: nowadays and way forward. *Int. Sh. Build Prog.* 60, 3–105.
- 654 Tezdogan, T., Incecik, A., Turan, O., 2016. Full-scale unsteady RANS simulations of vertical ship motions in shallow
655 water. *Ocean Eng.* 123, 131–145.
- 656 Tuck, E.O., 1964. A systematic asymptotic expansion procedure for slender ships. *J. Sh. Res.* 8, 15–23.
- 657 Tulin, M.P., Yao, Y., Wang, P., 2000. The generation and propagation of ship internal waves in a generally stratified
658 ocean at high densimetric Froude numbers, including nonlinear effects. *J. Sh. Res.* 44, 197–227.
- 659 Wurpts, R.W., 2005. 15 years experience with fluid mud: Definition of the nautical bottom with rheological parameters.
660 *Terra Aqua* 22–32.
- 661
- 662 Wurpts, R., 2005. 15 years' experience with fluid mud: definition of the nautical bottom with rheological parameters.
663 *Terra et Aqua.* 99
- 664 Zhao, F., Zhang, J., Hong, F.-W., Li, P., Yun, J., 2006. Numerical simulation of internal waves excited by a submarine
665 moving in the two-layer stratified fluid. *J. Hydrodyn. Ser. B* 18, 330–336.

666 **8 AUTHORS BIOGRAPHY**

667 **Sami Kaidi** holds the current position of researcher at Centre for Studies and Expertise on Risks, Environment, Mobili-
668 ty, and Urban and Country Planning. Hi is responsible for Ship Hydrodynamic and Manoeuvring researches. His previ-
669 ous experience includes: CFD method; Fluid-structure interaction, numerical methods,

670

671 **Emmanuel Lefrançois** holds the current position of Professor at University of Technology of Compiègne. Hi is respon-
672 sible for Fluid-structure interaction researches. His previous experience includes: the fluid-structure interaction methods
673 and the development of innovative numerical methods for engineering problems.

674

675 **Hassan Smaoui** holds the current position of research director at Centre for Studies and Expertise on Risks, Environ-
676 ment, Mobility, and Urban and Country Planning. He is responsible for laboratory of numerical hydraulic. His previous
677 experience includes: the sedimentary transport, the bank erosion and finite element method.